Hindawi
Journal of Sensors
Volume 2021, Article ID 5599096, 23 pages
https://doi.org/10.1155/2021/5599096

Research Article

Signal Denoising Based on Wavelet Threshold Denoising and Optimized Variational Mode Decomposition

Hongping Hu, Yan Ao, Huichao Yan, Yanping Bai, and Na Shi

School of Science, North University of China, Taiyuan, Shanxi, China 030051

Correspondence should be addressed to Hongping Hu; hhp92@163.com

Received 5 February 2021; Revised 11 March 2021; Accepted 1 April 2021; Published 14 July 2021

Academic Editor: Giovanni Diraco

To eliminate the noise from the signals received by MEMS vector hydrophone, a joint algorithm is proposed in this paper based on wavelet threshold (WT) denoising, variational mode decomposition (VMD) optimized by a hybrid algorithm of Multiverse Optimizer (MVO) and Particle Swarm Optimization (PSO), and correlation coefficient (CC) judgment to perform the signal denoising of MEMS vector hydrophone, named as MVO-PSO-VMD-CC-WT, whose fitness function is the root mean square error (RMSE) and whose individual is the parameters of VMD. For every individual, the original signal is decomposed by VMD into pure components, noisy components, and noise components in terms of CC judgment, where the pure components are directly retained, the noisy components are denoised by WT denoising, and the noise components are discarded, and then, the denoised noisy components and the pure components are reconstructed to be the denoised signal of the original signal. Then, the obtained optimal individual is utilized to perform the signal denoising by MVO-PSO-VMD-CC-WT by the use of the above repeated signal processing. Two simulated experimental results show that the MVO-PSO-VMD-CC-WT algorithm which has the highest signal-to-noise ratio and the least RMSE is superior to the other compared algorithms. And the proposed MVO-PSO-VMD-CC-WT algorithm is effectively applied to perform the signal denoising of the actual lake experiments. Therefore, the proposed MVO-PSO-VMD-CC-WT is suitable for the signal denoising and can be applied into the actual experiments in signal processing.

1. Introduction

There are rich resources in the marine environment, which are an important treasure trove to have influences on human development in the future [1, 2]. More and more people have devoted to detecting the ocean and continually seeking the acoustic wave detection technology with long propagation distance, fast propagation speed, and small energy loss. A MEMS hydrophone [3] is an important tool to be applied to receive the underwater signal. The state parameters such as the target category, the relative angle, and the position of the sound source are obtained by processing the received signal. However, there exists the complex environment in the ocean, which leads to the complex acoustic wave. The received signals from the MEMS hydrophone are that the target signals are inevitably mixed with different noises, such as biological noise, background noise, and tugboat noise. Therefore, it is necessary to denoise the signal to better understand the target signal and to apply the signal in a wider range, such as signal positioning, fault diagnosis, and analysis [4].

The concrete details of the signals cannot be obtained by the traditional Fourier transform [5], but the frequency components of known signals can only be obtained and the time of each component is unknown, which causes the time-frequency description and noise reduction effect of the non-stationary signal to be worse. The short-time Fourier transform [6] overcomes the shortcomings of the worst local analysis on signal by the traditional Fourier transform [7], but it cannot achieve fast analysis on signal. Wavelet analysis [8] with the characteristics of multiresolution analysis is a time-frequency analysis method and can analyze the time-frequency and frequency domain of the signal at the same time, which has been widely used in many fields. It is more suitable to analyze and process nonstationary signals and can better distinguish the abrupt parts of the signal and noise to perform the signal denoising. In [9], the wavelet packet

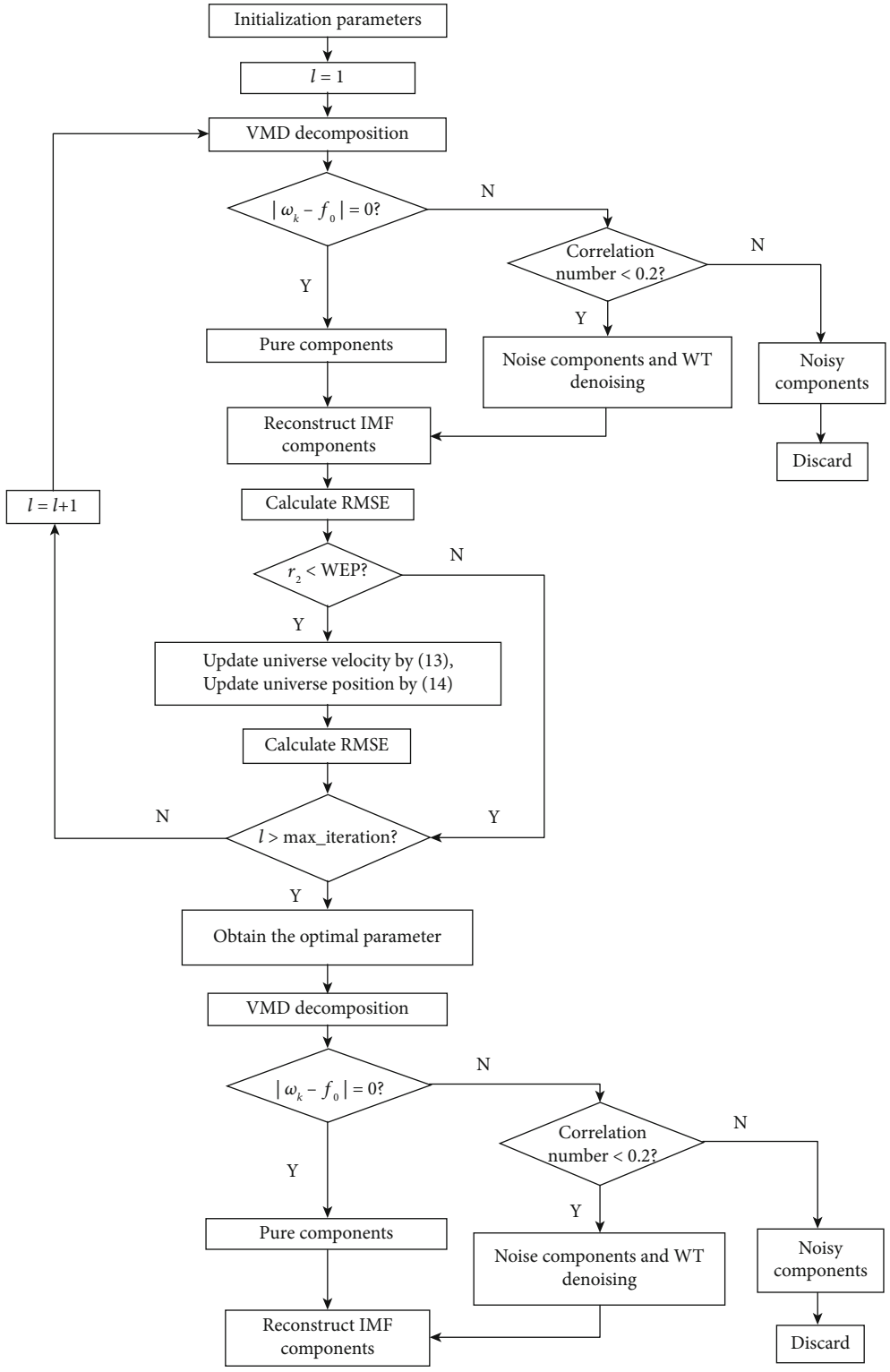

Figure 1: The flowchart of MVO-PSO-VMD-CC-WT.

transformation method can be applied to the structural characteristics of signal location by mathematical induction. In [10], wavelet packet to scan probe microscope is applied to improve the quality of scanning images and the control system strategy. In [11], a biorthogonal wavelet tree is applied to perform intelligent sensor embedded signal classification. Meanwhile, wavelet analysis also has been one of the most commonly used methods for underwater acoustic signal denoising. According to the different basis, the corresponding wavelet function is obtained. The Haar wavelet is the simplest wavelet function and discontinuous in the time domain; the Mexican hat wavelets and Morlet wavelets do not have

scale functions and not orthogonal; the Meyer wavelet is not tightly supported; the Daubechies wavelet is finite in the time domain and often used to decompose and reconstruct the signals as filters. In this paper, the Daubechies wavelet is chosen to be the wavelet base.

Empirical Mode Decomposition (EMD) proposed in 1988 [12] is a new time-frequency analysis method, which can adaptively decompose nonlinear and nonstationary signals to perform the signal processing and has been widely applied in many areas, such as seismic signal [13], speech recognition [14], and bearing fault diagnosis [15]. According to the local characteristics of the time scale of the signal, EMD can decompose the signal into a finite number of intrinsic modal functions (IMFs) from high frequencies to low frequencies. But there exists mode aliasing in the decomposed IMF layer, where two adjacent inherent modal function waveforms are aliased to cause a large amount of noise mixed in the reconstructed signal. An Ensemble Empirical Mode Decomposition (EEMD) method [16] was proposed by auxiliary noise being added into the original signal to improve the influence of modal aliasing [17]. However, the signal decomposed by the EEMD method contains residual noise, which leads to a large error when reconstructing the signal. Based on the theory of EEMD, Yeh et al. proposed a Complete Ensemble Empirical Mode Decomposition (CEEMD) method [18]. In the CEEMD method, the auxiliary noises in the form of positive and negative pairs are added into the signal, which can not only eliminate residual auxiliary noise but also effectively reduce the number of added noise sets [19]. However, the IMFs of each signal decomposition in the CEEMD method are different, which results in randomness of signal decomposition.

Variational mode decomposition (VMD) proposed in 2014 [20] is an adaptive nonrecursive signal processing algorithm, which has been applied into many different areas. Different from EMD, EEMD, and CEEMD, VMD has a solid theoretical foundation and can better solve modal aliasing problems [21]. In [21], VMD is used to be combined with wavelet denoising algorithm for performing the underwater acoustic signal denoising, but the number k of IMFs obtained by VMD and the penalty factor α need to be set up in advance. These two parameters k and α directly affect the final decomposition results: less k will cause insufficient signal decomposition, while excessive k will produce some false components which will interfere with the analysis of the useful components of the original signal; excessive α will make the modal broadband smaller, while less α will make the modal broadband larger. Therefore, the appropriate parameters k and α are the essential key in VMD for signal decomposition. In addtion,in [22–24], VMD has been applied into the seismic data analysis. In [25], VMD is also applied to preform fault diagnosis.

In recent years, some researches only have been done to optimize the number k of IMFs. For example, if the difference between the mutual information obtained from the reconstructed sequence signal by VMD and the original signal when $k = k_i$ and $k = k_{i+1}$ is less than the threshold, $k = k_i$ is chosen to be the appropriate number of IMFs in VMD [26]; the orthogonal value is calculated in terms of the length of data, and the optimal k is to be the value corresponding to the minimum orthogonal value [27]; an adaptive parameter optimized VMD method proposed determines the optimal parameter k by judging the ratio of the center frequencies of two adjacent IMFs [28].

Table 1: Initial parameters of MVO-PSO-VMD-CC-WT.

Parameter	Value or region
Number k of IMFs	$k \in [3, 10],\ k \in Z$
Penalty factor α	$\alpha \in [3000, 5000],\ \alpha \in Z$
The maximum iteration number: Maxgen	30
The size of population	20
Acceleration factor c_1	2
Acceleration factor c_2	2
Inertia weight ω	$e^{-(l/\text{Maxgen})}$, where l is the current iteration and Maxgen is the maximum iteration

Some researches have also been performed to optimize both these two parameters k and α of VMD. In particular, the proposed intelligence algorithms are utilized to obtain the optimal parameters k and α of VMD. For instance, in [29], genetic algorithm is employed to optimize k and α by taking the envelope entropy as the fitness function, in [30], whale optimization algorithm is used to optimize k and α by taking the power spectral entropy (PSE) as the fitness function, and in [31], spectral aggregation factor method is proposed to adjust penalty factor adaptively.

To eliminate the noise from the signals received by MEMS vector hydrophone, a joint algorithm is proposed in this paper based on wavelet threshold (WT) [21] denoising, VMD optimized by a hybrid algorithm of Multiverse Optimizer (MVO) [32] and Particle Swarm Optimization (PSO) [33], and correlation coefficient (CC) [34] judgment to perform the signal denoising of MEMS vector hydrophone, named as MVO-PSO-VMD-CC-WT, whose fitness function is the root mean square error (RMSE) and whose individual is the parameters of VMD. For every individual, the original signal is decomposed by VMD into pure components, noisy components, and noise components (similar to those in [21]) in terms of CC judgment, where the pure components are directly retained, the noisy components are denoised by WT denoising, and the noise components are discarded, and then, the denoised noisy components and the pure components are reconstructed to be the denoised signal of the original signal. Then, the obtained optimal individual is utilized to perform the signal denoising by MVO-PSO-VMD-CC-WT by the use of the repeated signal processing. Two simulated experimental results show that the proposed MVO-PSO-VMD-CC-WT algorithm which has the highest signal-to-noise ratio and the least RMSE is superior to the other compared algorithms. And the proposed MVO-PSO-VMD-CC-WT algorithm is effectively applied to perform the signal denoising of the actual lake experiments. Therefore, the proposed MVO-PSO-VMD-CC-WT algorithm is suitable for the signal denoising and

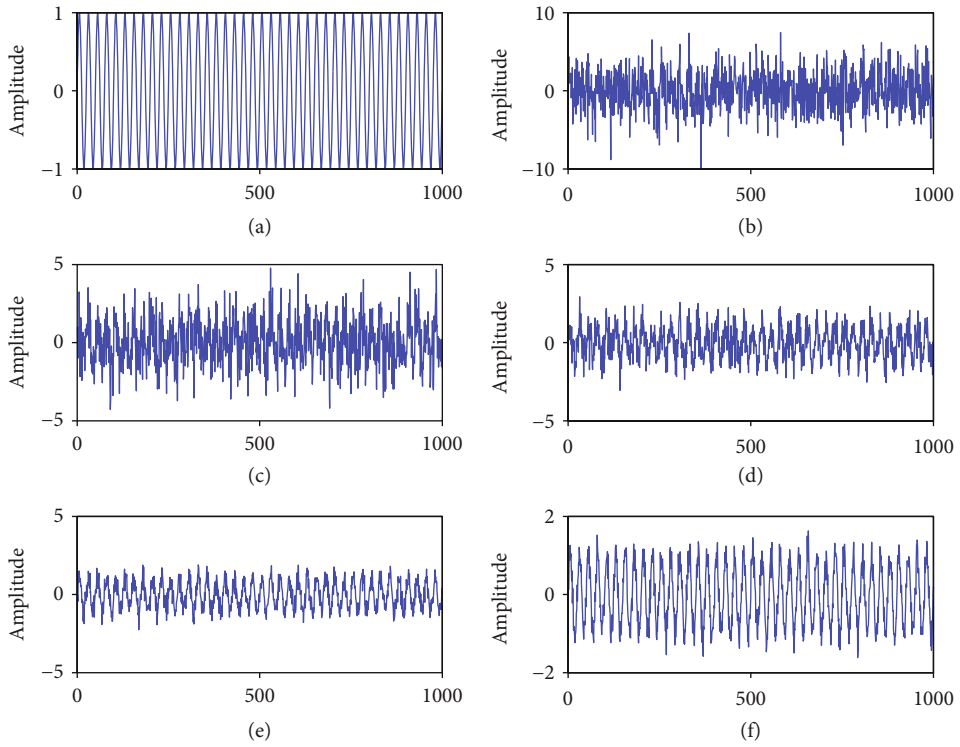

Figure 2: Source signal and five kinds of noisy signal. (a) The source signal. (b) The noisy signal under -10 dB. (c) The noisy signal under -5 dB. (d) The noisy signal under 0 dB. (e) The noisy signal under 5 dB. (f) The noisy signal under 10 dB.

can be applied into the actual experiments in signal processing.

The rest of this paper is organized as follows. In Section 2, VMD, WT denoising, MVO, PSO, and CC are introduced in detail. In Section 3, the hybrid MVO-PSO-VMD-CC-WT is proposed. In Section 4, two kinds of simulated signals are given to verify the validation of the proposed MVO-PSO-VMD-CC-WT. In Section 5, the proposed MVO-PSO-VMD-CC-WT is applied to perform the signal denoising on the Fenji Lake experimental data of North University of China. Conclusion and discussion are given in Sections 6 and 7, respectively.

2. The Basic Methods

2.1. Variational Mode Decomposition. Variational mode decomposition (VMD) [20] is an adaptive nonrecursive algorithm for signal processing, whose concrete steps are as follows.

Step 1. For every inherent modal function $u_k(t)$, Hilbert transform [33] is used to obtain the analytical signal of $u_k(t)$ as follows:

$$\left(\delta(t) + \frac{j}{\pi t}\right) u_k(t). \tag{1}$$

Step 2. The obtained analytical signal (1) is multiplied by an exponential term $e^{-j\omega t}$ to become the following:

$$\left[\left(\delta(t) + \frac{j}{\pi t}\right) u_k(t)\right] e^{-j\omega t}. \tag{2}$$

Thus, the spectrum of each modal function $u_k(t)$ is modulated to the corresponding baseband.

Step 3. By calculating the 2-norm square of (2), the bandwidth of every modal function $u_k(t)$ is estimated. Thus, the corresponding variation problem with constraints on the bandwidth is as follows:

$$\begin{aligned} &\min_{\{u_k\},\{\omega_k\}} \left\{ \sum_k \left\| \partial_t \left[\left(\delta(t) + \frac{j}{\pi t}\right) u_k(t) \right] e^{-j\omega t} \right\|_2^2 \right\} \\ &\text{s.t.} \quad \sum_k u_k(t) = f(t), \end{aligned} \tag{3}$$

where $\{u_k\} = \{u_1, \cdots, u_K\}$ and $\{\omega_k\} = \{\omega_1, \cdots, \omega_K\}$ are the sets of all modes and the corresponding central frequencies, respectively, $\delta(t)$ is a Dirichlet function, and ∂_t is the derivative with respect to time t.

The method to solve (3) is that the penalty factor α and Lagrange multiplier λ are introduced into (3) and (3) is transformed to be the unconstrained variation problem (4), as follows:

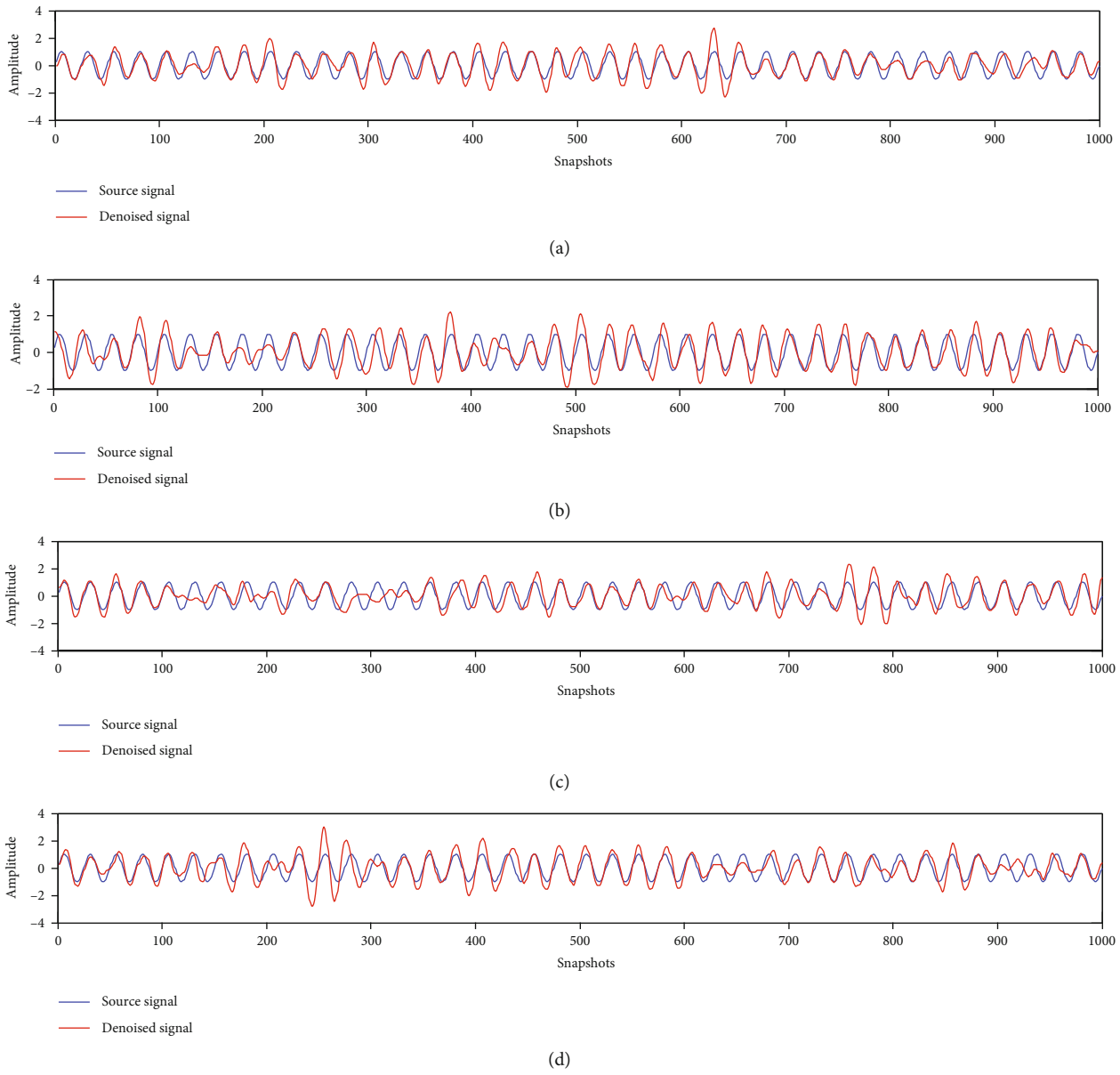

Figure 3: Denoised results of these four algorithms under -10 dB: (a) MVO-PSO-VMD-CC-WT; (b) MVO-VMD-CC-WT; (c) PSO-VMD-CC-WT; (d) VMD-CC-WT.

$$L(\{u_k\},\{\omega_k\},\lambda) = \alpha\sum_k \left\| \partial_t \left[\left(\delta(t) + \frac{j}{\pi t}\right) u_k(t) \right] e^{-j\omega t} \right\|_2^2 + \left\| f(t) - \sum_k u_k(t) \right\|_2^2 + \left\langle \lambda(t), f(t) - \sum_k u_k(t) \right\rangle. \tag{4}$$

The alternate direction method of multiplier (ADMM) is used to solve (4). Thus, the "saddle point" problem of Lagrange expression is solved by iterative update ways of u_k^{n+1}, ω_k^{n+1}, and λ^{n+1} whose expressions are as follows:

$$u_k^{n+1}(\omega) = \frac{f(\omega) - \sum_{i-1}^{k-1} u_i^{n+1}(\omega) - \sum_{i-k+1}^{K} u_i^n(\omega) + ((\lambda(\omega))/2)}{1 + 2\alpha(\omega - \omega_k^n)^2}, \tag{5}$$

$$\omega_k^{n+1} = \frac{\int_0^\infty \omega \left| u_k^{n+1}(\omega) \right|^2 d\omega}{\int_0^\infty \left| u_k^{n+1}(\omega) \right|^2 d\omega}, \tag{6}$$

$$\lambda^{n+1}(\omega) = \lambda^n(\omega) + \tau \left[f(\omega) - \sum_k u_k^{n+1}(\omega) \right], \tag{7}$$

where τ is the noise tolerance parameter, ω is the frequency, n is the current iteration, and $f(\omega)$ is the corresponding result of $f(t)$ obtained by Fourier transform.

Let ε be the convergence tolerance. The iteration terminates if and only if the iteration arrives at the maximum iteration or the condition $((\sum k \| u_k^{n+1}(\omega) - u_k^n(\omega) \|_2^2)/(\| u_k^n(\omega) \|_2^2)) < \varepsilon$ is satisfied.

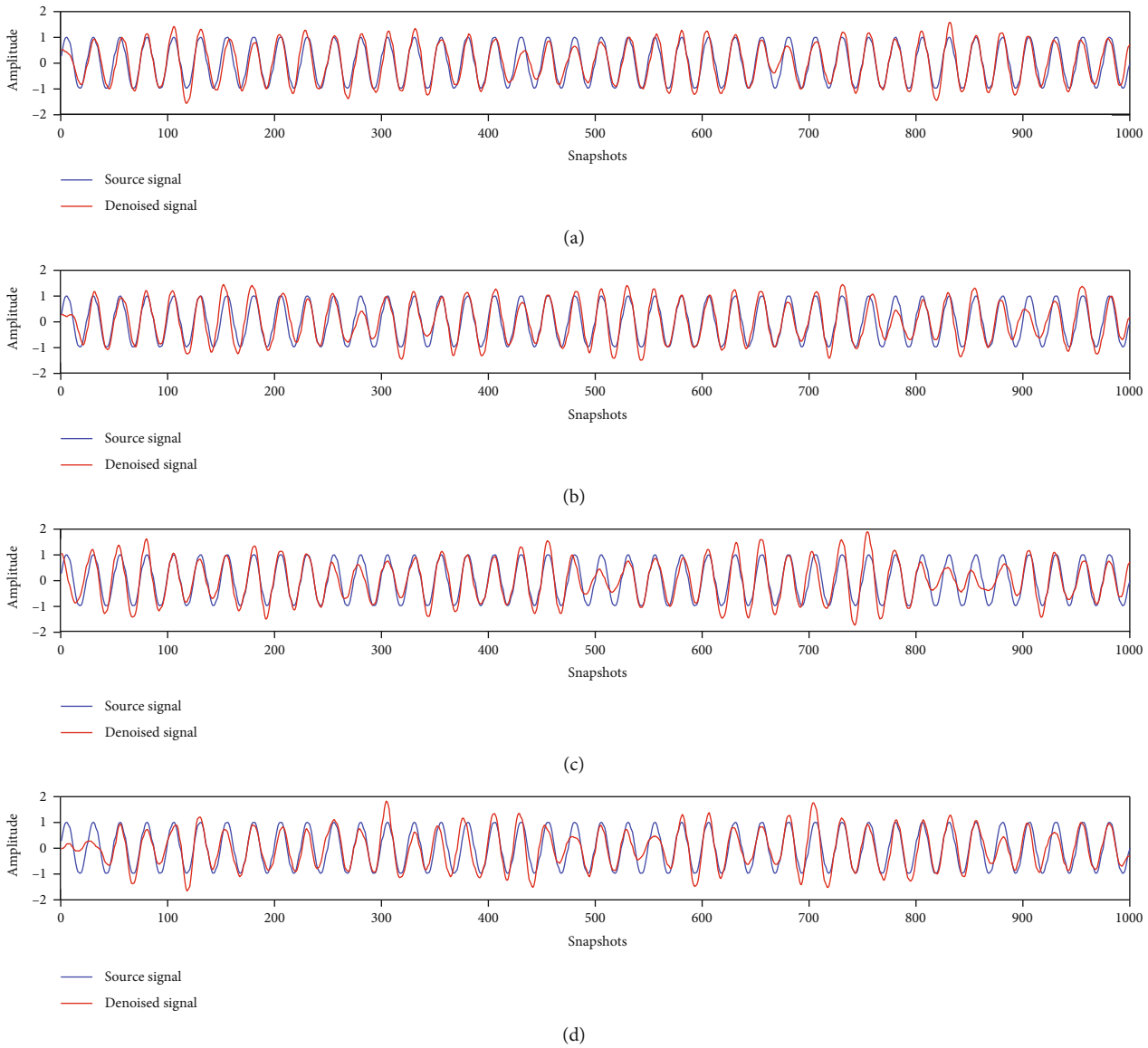

Figure 4: Denoised results of these four algorithms under -5 dB: (a) MVO-PSO-VMD-CC-WT; (b) MVO-VMD-CC-WT; (c) PSO-VMD-CC-WT; (d) VMD-CC-WT.

In the actual applications, two parameters τ and ε in VMD have little influence on the decomposition results, which causes that these parameters τ and ε in VMD are set up to be the same as those in Reference [21].

2.2. Wavelet Threshold Denoising. Wavelet transform is used to analyze the multilevel, low-frequency, and high-frequency signals, which is the key of the wavelet threshold (WT) [21] denoising. In this paper, the adopted WT denoising method is the soft threshold denoising method.

The soft threshold denoising method widely used in engineering is performed by setting up a threshold λ in advance. Let x be the wavelet coefficient obtained after orthogonal decomposition of the noisy signal and $f(x)$ be the eliminated wavelet coefficient of the actual signal. Thus, the relation between $f(x)$ and x is as follows:

$$f(x) = \begin{cases} \text{sgn}\,(x)(|x| - \lambda), & |x| > \lambda, \\ 0, & |x| \le \lambda, \end{cases} \tag{8}$$

where sgn $(\cdot)$ is a sign function and λ is a threshold. In general, the threshold λ is taken to be $\lambda = \sigma\sqrt{2 \log N}$, where σ is the standard deviation of noise and N is the signal length.

2.3. Multiverse Optimizer. Multiverse Optimizer (MVO) [32] proposed in 2016 is a new metaheuristic algorithm, which was inspired by the concepts of black holes, white holes, and wormholes based on the Big Bang theory. Black holes attract everything by their extremely high gravity; white holes send objects as the main components of the birth of the universe; wormholes are the holes connected with different components of the universes and act as the time/space travel

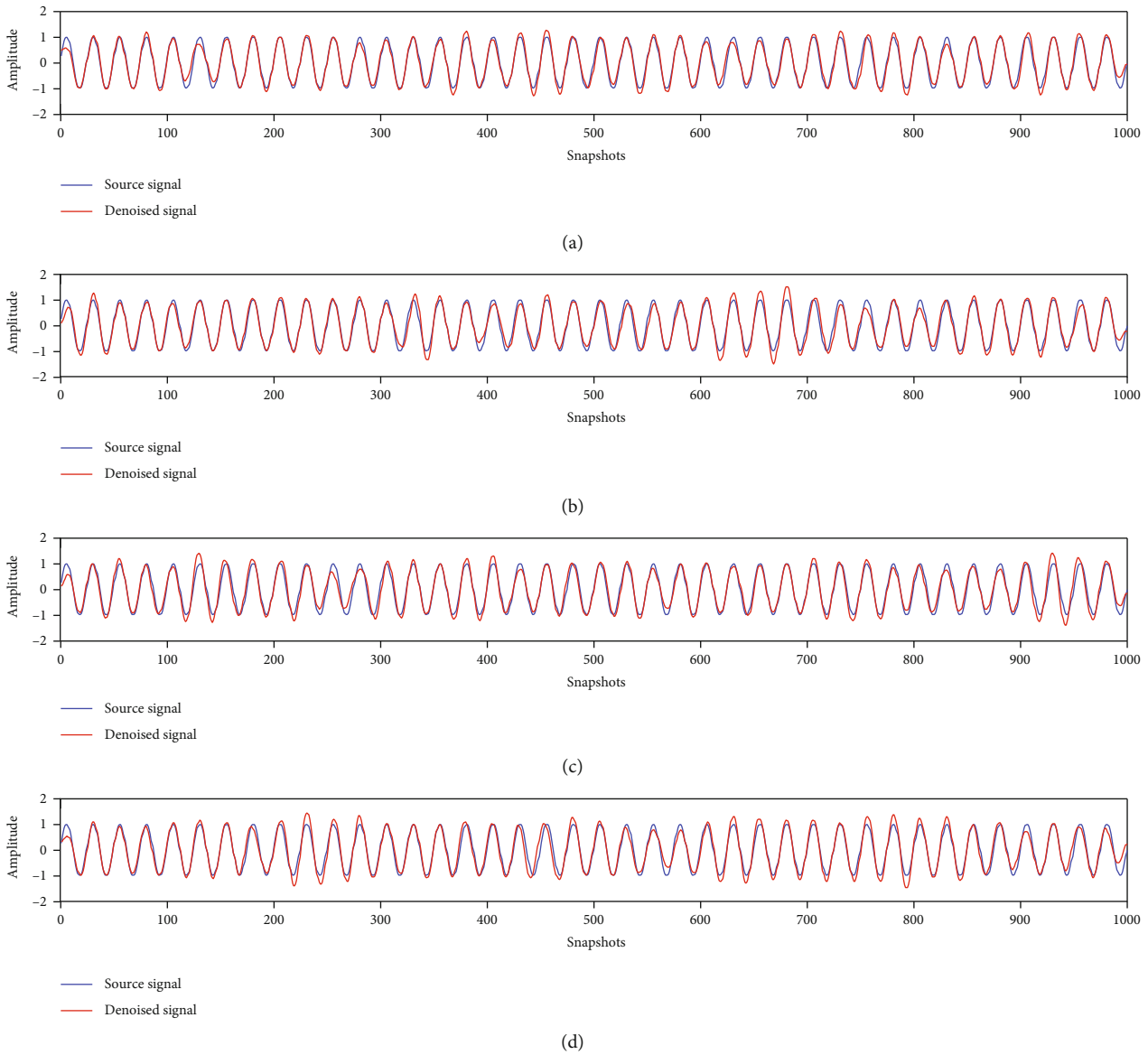

Figure 5: Denoised results of these four algorithms under 0 dB: (a) MVO-PSO-VMD-CC-WT; (b) MVO-VMD-CC-WT; (c) PSO-VMD-CC-WT; (d) VMD-CC-WT.

tunnels for sending the objects from one universe to another universe. In MVO, black holes and white holes represent the exploration stage, and wormholes represent the exploitation stage. Suppose that every solution is regarded to be one universe, and every component is regarded to be one object. And every solution has the corresponding inflation rate which is proportional to the fitness function.

Let $u_i = (x_{i1}, x_{i2}, \cdots, x_{id})\ (i = 1, 2, \cdots, n)$ be n universes, where x_{ij} is the j^{th} object of the i^{th} universe $u_i (j = 1, 2, \cdots, d)$. According to the roulette wheel selection mechanism,

$$x_{ij} = \begin{cases} x_{kj}, & r_1 < \text{NI}(u_i), \\ x_{ij}, & r_1 \geq \text{NI}(u_i), \end{cases} \tag{9}$$

where r_1 is a random number in $[0, 1]$, $\text{NI}(u_i)$ is normalized inflation rate of the i^{th} universe, and x_{kj} is the j^{th} object of the k^{th} universe selected according to the roulette mechanism.

Based on the above mechanism, the objects are changed between the universes without interference and the wormholes exist in every universe such that the objects are transformed between the universes though the wormholes. If the inflation rate is not considered, then the objects in the universe are randomly updated. Suppose that there exist wormhole tunnels between every universe and the optimal universe. Then,

$$x_{ij} = \begin{cases} X_j + \text{TDR} \times \left(\left(\text{ub}_j - \text{lb}_j \right) \times r_4 + \text{lb}_j \right) & r_3 < 0.5, \\ X_j - \text{TDR} \times \left(\left(\text{ub}_j - \text{lb}_j \right) \times r_4 + \text{lb}_j \right) & r_3 \geq 0.5, \\ x_{ij}, & \end{cases} \quad \begin{matrix} r_2 < \text{WEP}, \\ \\ r_2 \geq \text{WEP}, \end{matrix} \tag{10}$$

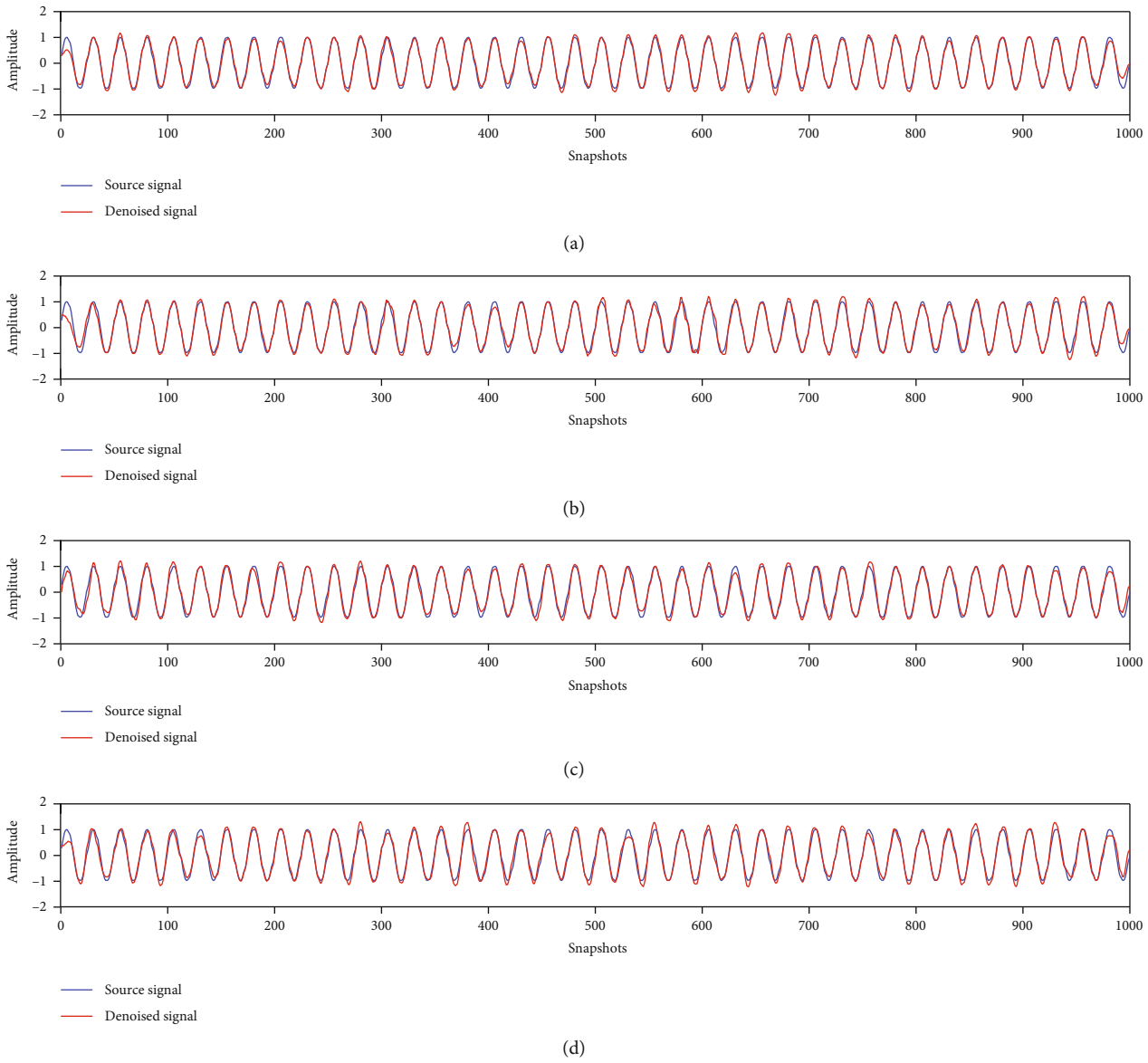

Figure 6: Denoised results of these four algorithms under 5 dB: (a) MVO-PSO-VMD-CC-WT; (b) MVO-VMD-CC-WT; (c) PSO-VMD-CC-WT; (d) VMD-CC-WT.

where X_j is the j^{th} object of the optimal universe, r_2, r_3, r_4 are the random numbers distributed in [0, 1], lb_j and ub_j are the lower bound and the upper bound of the j^{th} object, respectively, TDR is the travel distance rate, and WEP indicates the probability of wormhole existence.

WEP and TDR are defined as follows:

$$\text{WEP} = \min + (\max - \min) \times \frac{l}{L}, \tag{11}$$

$$\text{TDR} = 1 - \left(\frac{l}{L}\right)^{1/p}, \tag{12}$$

where min and max are the minimum value and the maximum value of WEP (min = 0.2 and max = 1 in the general), respectively, l is the current iteration, and L is the maximum iteration.

2.4. Particle Swarm Optimization. Particle Swarm Optimization (PSO) [33] proposed in 1995 simulates the birds' foraging behavior.

In PSO, a bird is regarded as a particle, which is a solution of the optimization problem. In the search space, every particle has its velocity and its position.

There are n particles in PSO, where the velocity and the position of the i^{th} particle are $X_i = (x_{i1}, x_{i2}, \cdots, x_{iD})$ and $V_i = (v_{i1}, v_{i2}, \cdots, v_{iD})$, respectively. The velocity and the position of the i^{th} particle are updated are as follows:

$$V_i^{k+1} = \omega V_i^k + c_1 r_1 \left(P_i^k - X_i^k\right) + c_2 r_2 \left(P_g^k - X_i^k\right), \tag{13}$$

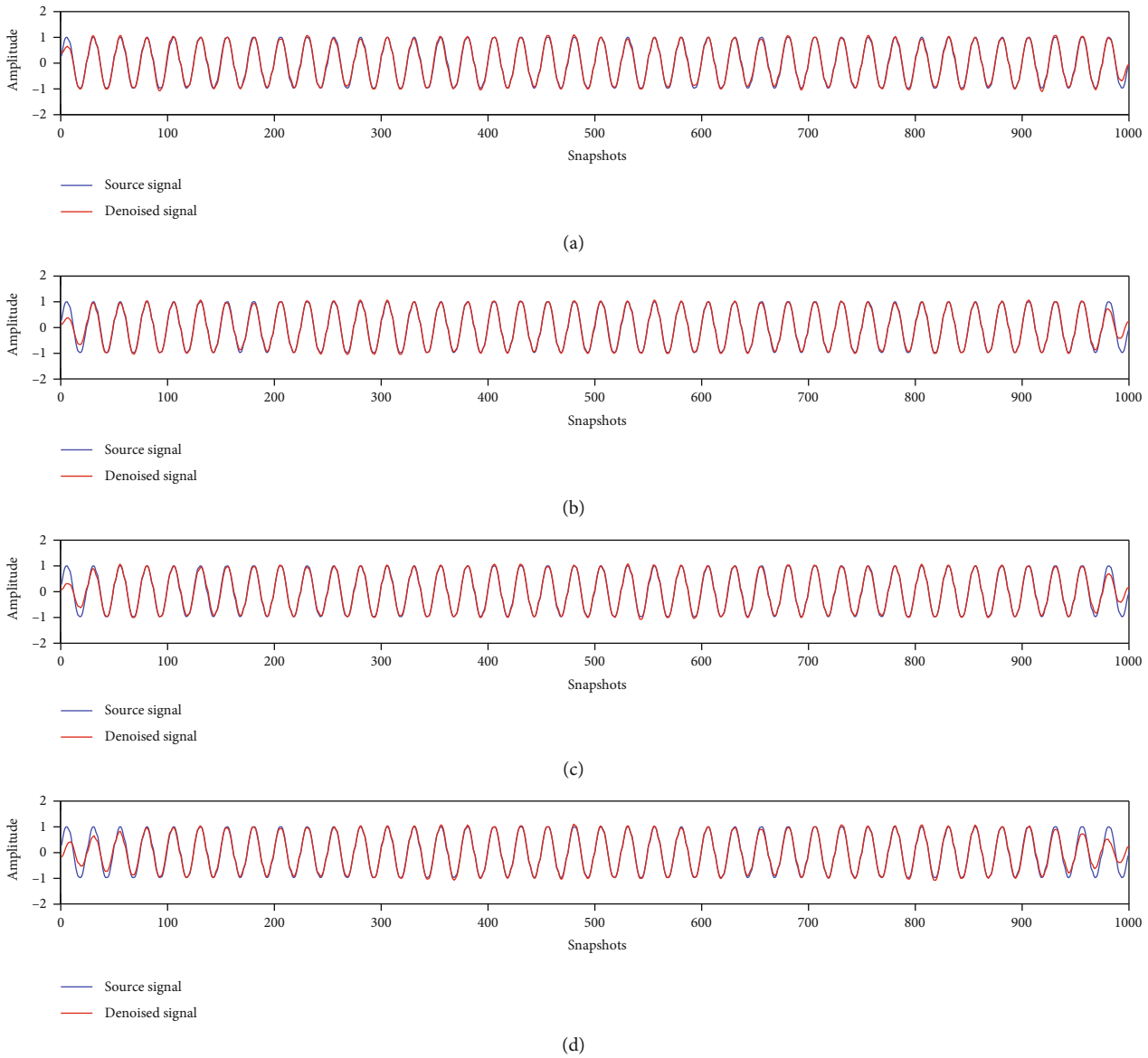

Figure 7: Denoised results of these four algorithms under 10 dB: (a) MVO-PSO-VMD-CC-WT; (b) MVO-VMD-CC-WT; (c) PSO-VMD-CC-WT; (d) VMD-CC-WT.

Table 2: The average SNRs and RMSEs obtained by five algorithms for Type I.

Noise intensity	Indicator	VMD-CC-WT	PSO-VMD-CC-WT	MVO-VMD-CC-WT	MVO-PSO-PSE-VMD-CC-WT	MVO-PSO-VMD-CC-WT
-10 dB	SNR	1.7290	1.9160	1.9691	2.2135	**3.6344**
	RMSE	0.5624	0.5624	0.5065	0.5477	**0.4661**
-5 dB	SNR	6.0429	6.6372	6.7344	7.0128	**8.6337**
	RMSE	0.3529	0.3297	0.3258	0.3156	**0.2618**
0 dB	SNR	11.2016	11.4757	11.9285	12.1574	**13.6008**
	RMSE	0.1952	0.1892	0.1794	0.1747	**0.1477**
5 dB	SNR	14.3201	14.9929	15.1734	15.3029	**17.0212**
	RMSE	0.1362	0.1225	0.1235	0.1217	**0.0998**
10 dB	SNR	14.9307	17.8312	18.1929	18.3556	**20.3457**
	RMSE	0.1267	0.0932	0.0872	0.0856	**0.0679**

Table 3: The average SNRs and RMSEs obtained by five algorithms for Type II.

Noise intensity	Indicator	VMD-CC-WT	PSO-VMD-CC-WT	MVO-VMD-CC-WT	MVO-PSO-PSE-VMD-CC-WT	MVO-PSO-VMD-CC-WT
-10 dB	SNR	1.5658	1.9283	1.9501	2.2377	**4.3433**
	RMSE	0.5907	0.5675	0.4963	0.5342	**0.4293**
-5 dB	SNR	6.1526	6.2342	6.4713	7.0062	**9.0947**
	RMSE	0.3489	0.3453	0.3361	0.3161	**0.2236**
0 dB	SNR	11.1970	11.2424	11.5588	11.9457	**13.8305**
	RMSE	0.1950	0.1942	0.1849	0.1777	**0.1440**
5 dB	SNR	14.0095	14.7189	15.0088	15.3264	**16.9478**
	RMSE	0.1409	0.1299	0.1258	0.1210	**0.1005**
10 dB	SNR	14.6676	17.4848	17.7375	18.2819	**20.1053**
	RMSE	0.1306	0.0945	0.0923	0.0862	**0.0695**

$$X_i^{k+1} = X_i^k + V_i^{k+1}, \tag{14}$$

where k is the current iteration, ω is the inertial weight, c_1 and c_2 are the acceleration factors, r_1 and r_2 are the random numbers distributed in [0, 1], P_i^k is the local optimal position of the i^{th} particle, and P_g^k is the global optimal position of all the particles.

2.5. Correlation Coefficient. The correlation coefficient (CC) [30] is an important parameter in statistics, which can measure the correlation between the denoised signal and the original signal. CC can distinguish whether the signal components obtained by VMD contain the main characteristics of the original signal for performing the signal denoising. The correlation coefficient R between the original signal and the IMFs is defined as follows:

$$R = \frac{E[u_k(t)f(t)] - E[u_k(t)]E[f(t)]}{\sqrt{D[u_k(t)]}\sqrt{D[f(t)]}}, \tag{15}$$

where $f(t)$ and $u_k(t)$ are the original signal and the k^{th} IMF component, respectively, and $E(\cdot)$ and $D(\cdot)$ are the mathematical expectation and variance of the signal, respectively.

3. The Proposed Signal Denoising Algorithm

3.1. MVO-PSO Algorithm. Owing to the constant movement of the universe, every universe has its velocity and position in the space. Therefore, the velocity of every universe is updated as Equation (13) of PSO, and the position of every universe based on Equation (10) of MVO is defined as follows:

$$x_{ij} = \begin{cases} X_j + V_{ij} + \text{TDR} \times \left(\left(\text{ub}_j - \text{lb}_j\right) \times r_4 + \text{lb}_j\right) & r_3 < 0.5, \\ X_j + V_{ij} - \text{TDR} \times \left(\left(\text{ub}_j - \text{lb}_j\right) \times r_4 + \text{lb}_j\right) & r_3 \geq 0.5, \\ x_{ij}, & \end{cases} \quad \begin{matrix} \\ r_2 < \text{WEP}, \\ \\ r_2 \geq \text{WEP}. \end{matrix} \tag{16}$$

Thus, the hybrid algorithm based on the combination of MVO and PSO is established, written as MVO-PSO.

3.2. MVO-PSO-VMD-CC-WT Algorithm. In this paper, two parameters (k, α) of VMD where k is the number of IMFs and α is the penalty factor are regarded to be a universe of MVO-PSO. And the root mean square error (RMSE)

$$\text{RMSE} = \sqrt{\frac{1}{N}\sum_{n=1}^{N}\left(x(n) - x'(n)\right)^2} \tag{17}$$

between the denoised signal obtained by VMD algorithm and the original signal is taken to be the fitness function of MVO-PSO, where $x'(n)$ and $x(n)$ are the denoised signal and the original signal, respectively, and N is the number of the snapshots.

Based on the above, a hybrid denoising method is proposed based on VMD, WT denoising, MVO-PSO, and CC in this paper, named as MVO-PSO-VMD-CC-WT. The flowchart of MVO-PSO-VMD-CC-WT is shown in Figure 1, and the steps of MVO-PSO-VMD-CC-WT are as follows.

Step 1. Initialize the parameters, shown in Table 1. Every individual (k, α) in MVO-PSO-VMD-CC-WT denotes a universe. And initialize the population of MVO-PSO. Let $l = 1$.

Step 2. Judge that the terminal condition is satisfied or the Maxgen is arrived. If yes, then turn Step 7; otherwise, turn Step 3.

Step 3. For every universe (k, α), VMD makes the original signal $s(n)$ be the component to be k IMFs. The main frequency f_0 of the original signal, the center frequency f_k of each IMF, and CC are calculated. The IMF whose center frequency f_k is the closest to the main frequency f_0 is regarded to be the pure IMF. Besides, the indicator of CC is 0.2, which is the same as that of Ref. [35]. The IMF whose CC is less than 0.2 is regarded to be the noise component, and the IMF whose CC is larger than 0.2 is regarded to be the noisy component. Thus, these IMFs are divided into pure IMFs, noisy IMFs, and noise IMFs in terms of CC.

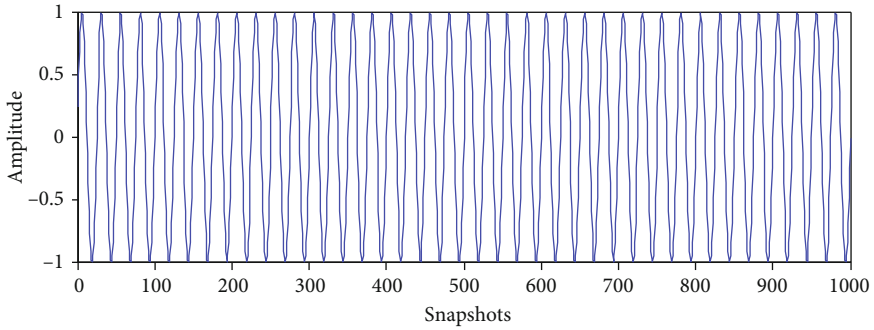

(a)

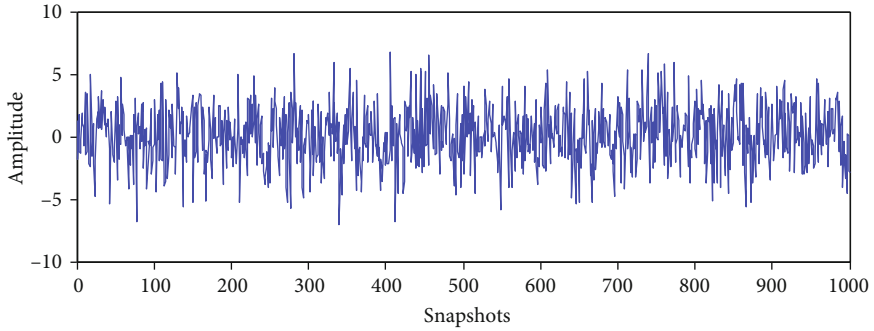

(b)

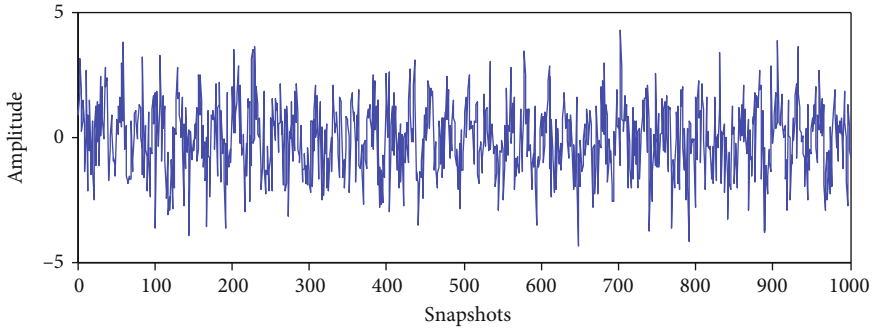

(c)

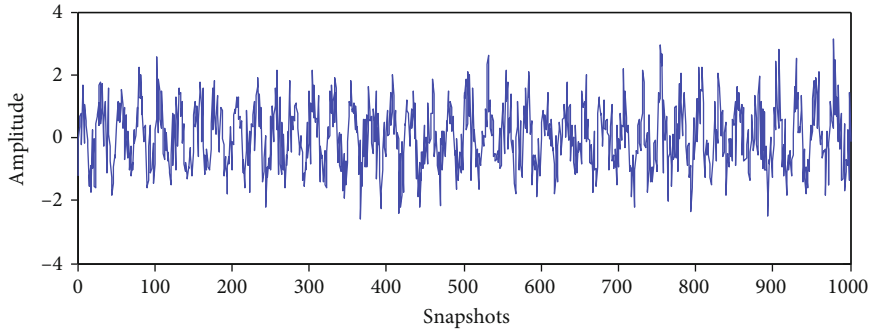

(d)

Figure 8: Continued.

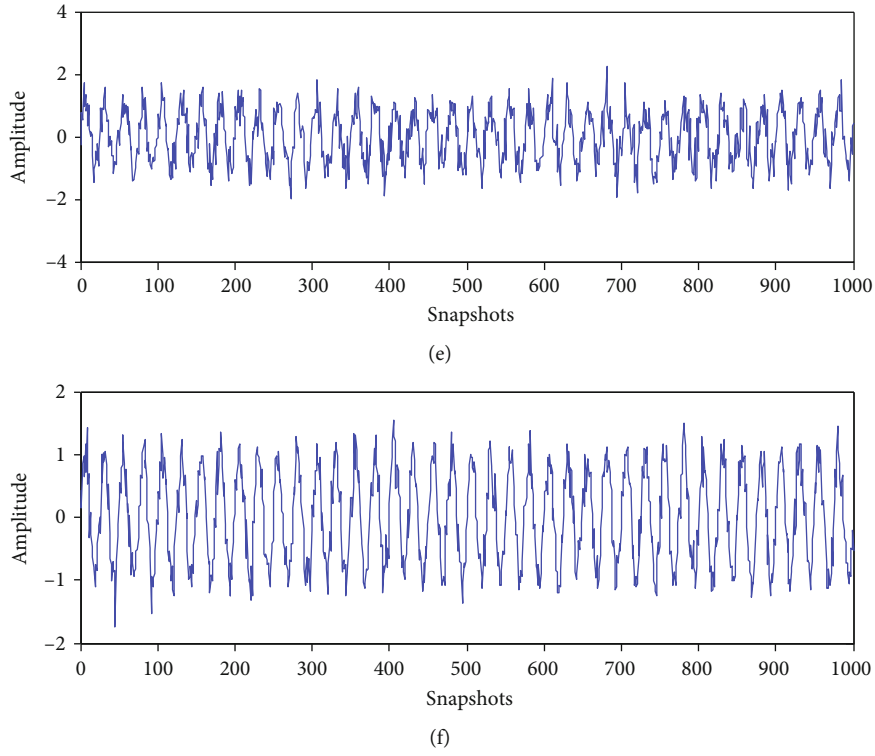

Figure 8: Source signal and five kinds of noisy signal. (a) The source signal. (b) The noisy signal under -10 dB. (c) The noisy signal under -5 dB. (d) The noisy signal under 0 dB. (e) The noisy signal under 5 dB. (f) The noisy signal under 10 dB.

Step 4. The pure IMFs are directly retained, the noisy IMFs are denoised by WT denoising, and the noise IMFs are discarded.

Step 5. The denoised noisy components and the pure components are reconstructed to be the denoised signal of the original signal. Then, the fitness value of this universe (k, α) is calculated in terms of Equation (17). Then, the global optimal universe of all the universes and the local best universe of every universe are obtained.

Step 6. For every universe (k, α), the velocity and the position of this universe are updated in MVO-PSO according to Equations (13) and (16). According to the upper and lower bounds of the components, the velocity and the position of this universe are further updated. Then, $l = l + 1$. Turn Step 2.

Step 7. For the global optimal universe (k, α) obtained from the MVO-PSO-VMD-CC-WT, perform Steps 3–5 and obtain the denoised signal of the original signal.

4. Simulated Experiments

Owing to the marine environment and human activities in the ocean exploration, the noise intensity of the underwater acoustic signal is constantly variable. In this section, the simulated signal with noise is defined as follows:

$$f(n) = s(n) + \mathrm{gs}(n), \tag{18}$$

where $f(n)$ is a noisy signal, $s(n)$ is a noise-free source signal, $\mathrm{gs}(n)$ is white Gaussian noise with different noise-added decibels, n is the sampling point, and N is the number of snapshots. In this section, $N = 1000$.

According to the complex underwater environment, we take two types of $s(n)$ to quantitatively evaluate the denoising performance of MVO-PSO-VMD-CC-WT.

For Type I, the noise-free source signal $s(n)$ is chosen to be a sinusoidal sequence signal defined as

$$s(n) = \sin\left(2\pi \cdot 40 \cdot n\right), \tag{19}$$

whose amplitude and frequency are 1 and 40 Hz, respectively.

For Type II, the noise-free source signal $s(n)$ is chosen to be a mixed frequency sequence signal defined as

$$s(n) = \sin\left(2\pi \cdot 40 \cdot n\right) + \sin\left(2\pi \cdot 400 \cdot n\right), \tag{20}$$

which is a mix of 40 Hz and 500 Hz frequencies.

In this paper, the signal-to-noise ratio (SNR) defined as

$$\mathrm{SNR} = 10 \cdot \log\left(\frac{\sum_{n=1}^{N} x^2(n)}{\sum_{n=1}^{N}\left[x(n) - x'(n)\right]^2}\right) \tag{21}$$

and RMSE defined as Equation (17) are used to be the denoised performance indicators, where $x'(n)$ and $x(n)$ are the denoised signal and the original signal, respectively, and

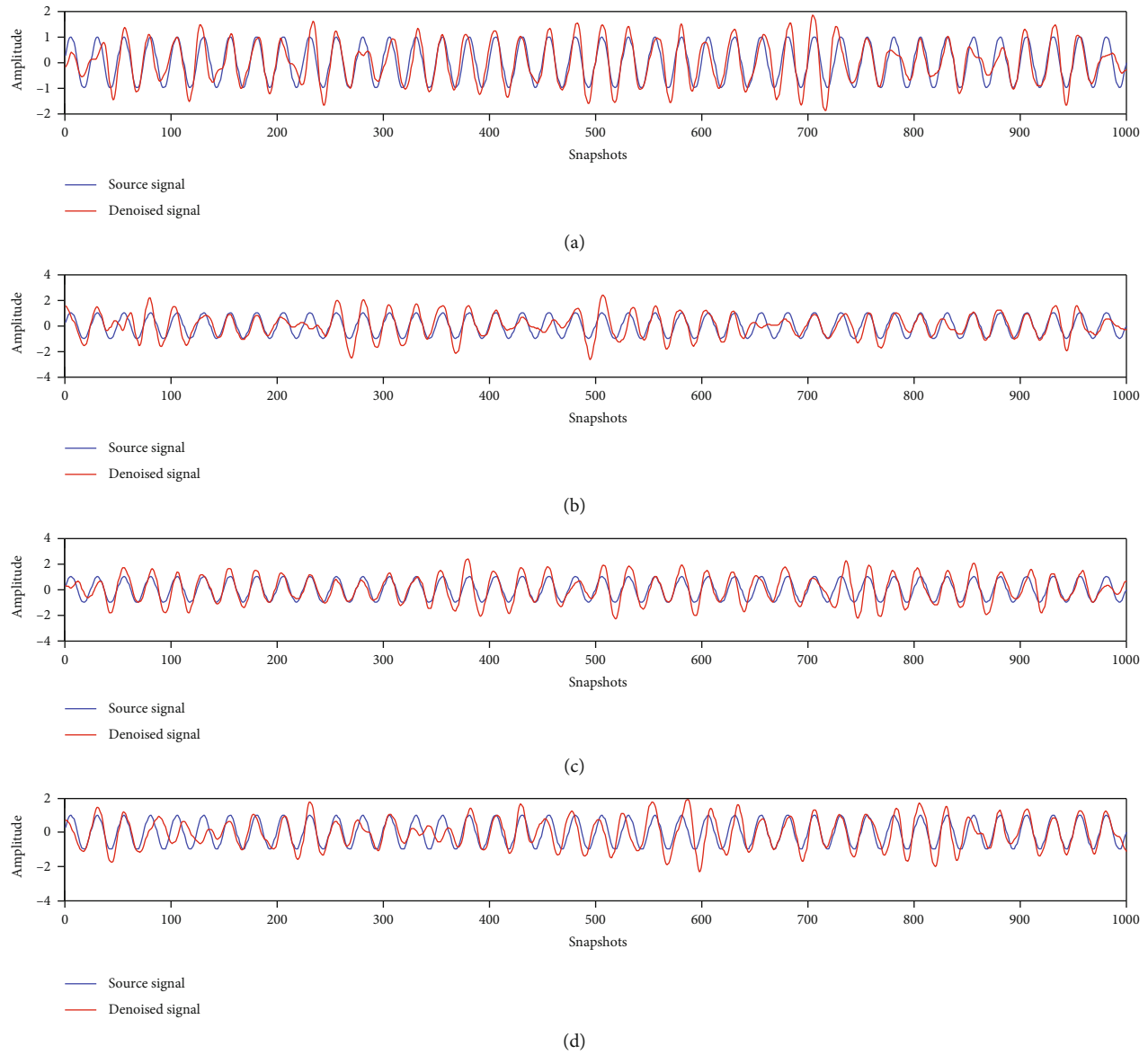

Figure 9: Denoised results of these four algorithms under -10 dB: (a) MVO-PSO-VMD-CC-WT; (b) MVO-VMD-CC-WT; (c) PSO-VMD-CC-WT; (d) VMD-CC-WT.

N is the number of snapshots. The higher the SNR is, the better the denoising effect is. And the smaller the RMSE is, the better the denoising effect is.

In this paper, VMD-CC-WT, PSO-VMD-CC-WT, and MVO-VMD-CC-WT are employed to be compared with MVO-PSO-VMD-CC-WT. Among these four algorithms, VMD-CC-WT, PSO-MD-CC-WT, MVO-VMD-CC-WT, and MVO-PSO-VMD-CC-WT, the fitness functions are all taken to be Equation (17).

4.1. Simulated Experiment for Type I. For the simulated signal of Type I whose noise-free source signal $s(n)$ is taken to be Equation (19), $\mathrm{gs}(n)$ is white Gaussian noise with noise-added -10 dB, -5 dB, 0 dB, 5 dB, and 10 dB, respectively. Thus, five kinds of noisy signals are obtained, shown in Figure 2. The denoised results of VMD-CC-WT, PSO-VMD-CC-WT, MVO-VMD-CC-WT, and MVO-PSO-VMD-CC-WT are shown in Figures 3–7 under -10 dB, -5 dB, 0 dB, 5 dB, and 10 dB, respectively.

From Figures 3–7, it is observed that all of these four algorithms VMD-CC-WT, PSO-VMD-CC-WT, MVO-VMD-CC-WT, and MVO-PSO-VMD-CC-WT have the abilities in performing the signal denoising of the simulated signal defined by Equations (18) and (19) where $\mathrm{gs}(n)$ is white Gaussian noise with noise-added -10 dB, -5 dB, 0 dB, 5 dB, and 10 dB. And it is observed that with the noise-added decibel increasing, the denoised signals obtained by these four algorithms match the source signal better and better. The denoised results show that MVO-PSO-VMD-CC-WT proposed in this paper is obviously superior to VMD-CC-WT, PSO-VMD-CC-WT, and MVO-VMD-CC-WT. And MVO-PSO-VMD-CC-WT has the ability in effectively eliminating the sharp burrs in the waveform of the denoised signal which becomes smoother and neater. In the

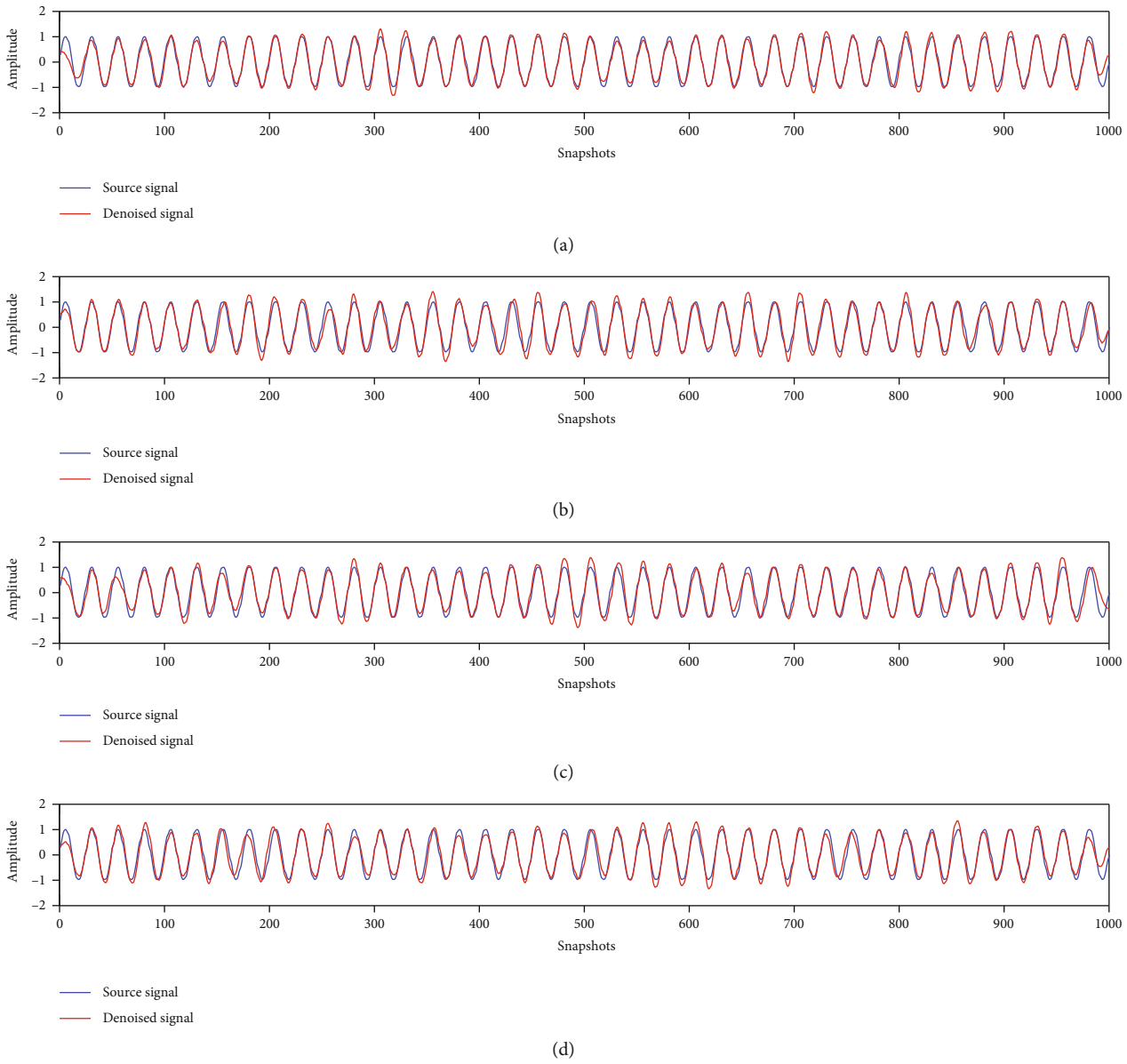

Figure 10: Denoised results of these four algorithms under -5 dB: (a) MVO-PSO-VMD-CC-WT; (b) MVO-VMD-CC-WT; (c) PSO-VMD-CC-WT; (d) VMD-CC-WT.

denoised signal obtained by the worst VMD-CC-WT, there exists the distortion on some local extremum points of the signal and the obvious concussion in the waveform, which illustrates that the parameters of VMD have the larger effect on the signal denoising. Compared with VMD-CC-WT, PSO-VMD-CC-WT and MVO-VMD-CC-WT improve the denoised results, but there exist the sharp protrusions in the denoised signal.

In order to further observe the compared results on the RMSE and SNR, we replace the fitness function of MVO-PSO-VMD-CC-WT with the power spectral entropy (PSE) introduced in Reference [30], named as MVO-PSO-PSE-VMD-CC-WT which is used to distinguish from MVO-PSO-VMD-CC-WT.

VMD-CC-WT, PSO-VMD-CC-WT, MVO-VMD-CC-WT, MVO-PSO-PSE-VMD-CC-WT, and MVO-PSO-VMD-CC-WT are independently run 30 times, respectively. The average SNRs and RMSEs are shown in Table 2.

From Table 2, it can be seen that MVO-PSO-VMD-CC-WT with different decibels has the least RMSE and the highest SNR among these five algorithms: SNR 3.6344 and RMSE 0.4661 under -10 dB; SNR 8.6337 and RMSE 0.2618 under -5 dB; SNR 13.6008 and RMSE 0.1477 under 0 dB; SNR 17.0212 and RMSE 0.0998 under 5 dB; SNR 20.3457 and RMSE 0.0679 under 10 dB. For the same decibels, according to the increasing of SNRs or the decreasing of RMSEs, the order of five algorithms in Table 3 is VMD-CC-WT, PSO-VMD-CC-WT, MVO-VMD-CC-WT, MVO-PSO-PSE-VMD-CC-WT, and MVO-PSO-VMD-CC-WT. And we also observe that SNRs are increasing and RMSEs are decreasing with the noise decibel increasing. Therefore, the results obtained from Table 2 show that MVO-PSO-VMD-CC-

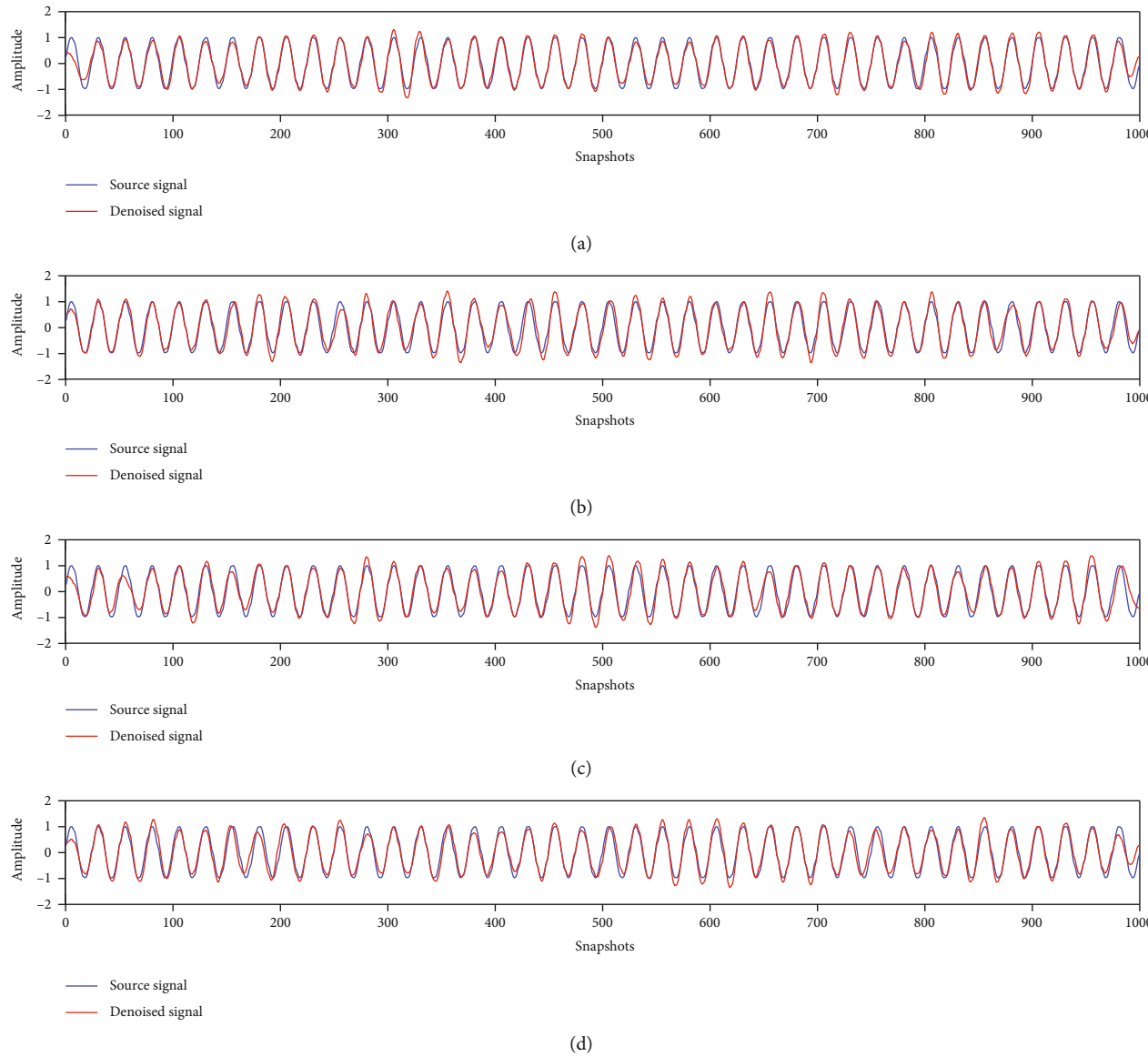

Figure 11: Denoised results of these four algorithms under 0 dB: (a) MVO-PSO-VMD-CC-WT; (b) MVO-VMD-CC-WT; (c) PSO-VMD-CC-WT; (d) VMD-CC-WT.

WT outperforms VMD-CC-WT, PSO-VMD-CC-WT, MVO-VMD-CC-WT, and MVO-PSO-PSE-VMD-CC-WT.

4.2. Simulated Experiment for Type II. In this section, the analyses are similar to the situation of Type I. For the simulated signal of Type II whose noise-free source signal $s(n)$ is taken to be Equation (20), $\mathrm{gs}(n)$ is also white Gaussian noise with noise-added -10 dB, -5 dB, 0 dB, 5 dB, and 10 dB, respectively. Thus, five kinds of noisy signals are obtained, shown in Figure 8. The denoised results of VMD-CC-WT, PSO-VMD-CC-WT, MVO-VMD-CC-WT, and MVO-PSO-VMD-CC-WT are shown in Figures 9–13 under -10 dB, -5 dB, 0 dB, 5 dB, and 10 dB, respectively.

From Figures 9–13, we also observe that all of these four algorithms VMD-CC-WT, PSO-VMD-CC-WT, MVO-VMD-CC-WT, and MVO-PSO-VMD-CC-WT have the abilities in performing the signal denoising of the simulated signal defined by Equations (18) and (20) where $\mathrm{gs}(n)$ is white Gaussian noise with noise-added -10 dB, -5 dB, 0 dB, 5 dB, and 10 dB. And it is observed that with the noise-added decibel increasing, the denoised signals obtained by these four algorithms match the source signal better and better.

From Figures 9–13, VMD-CC-WT has the worst denoising effect. Compared with VMD-CC-WT, PSO-VMD-CC-WT and MVO-VMD-CC-WT improve the denoising results, and the denoised signal waveform obtained by the MVO-VMD-CC-WT algorithm and PSO-VMD-CC-WT is smoother. Among these four algorithms VMD-CC-WT, PSO-VMD-CC-WT, MVO-VMD-CC-WT, and MVO-PSO-VMD-CC-WT, the denoised signal waveform obtained by MVO-PSO-VMD-CC-WT is the smoothest and the neatest and has the least distortion phenomenon.

Similar to the situation of Type I, VMD-CC-WT, PSO-VMD-CC-WT, MVO-VMD-CC-WT, MVO-PSO-PSE-

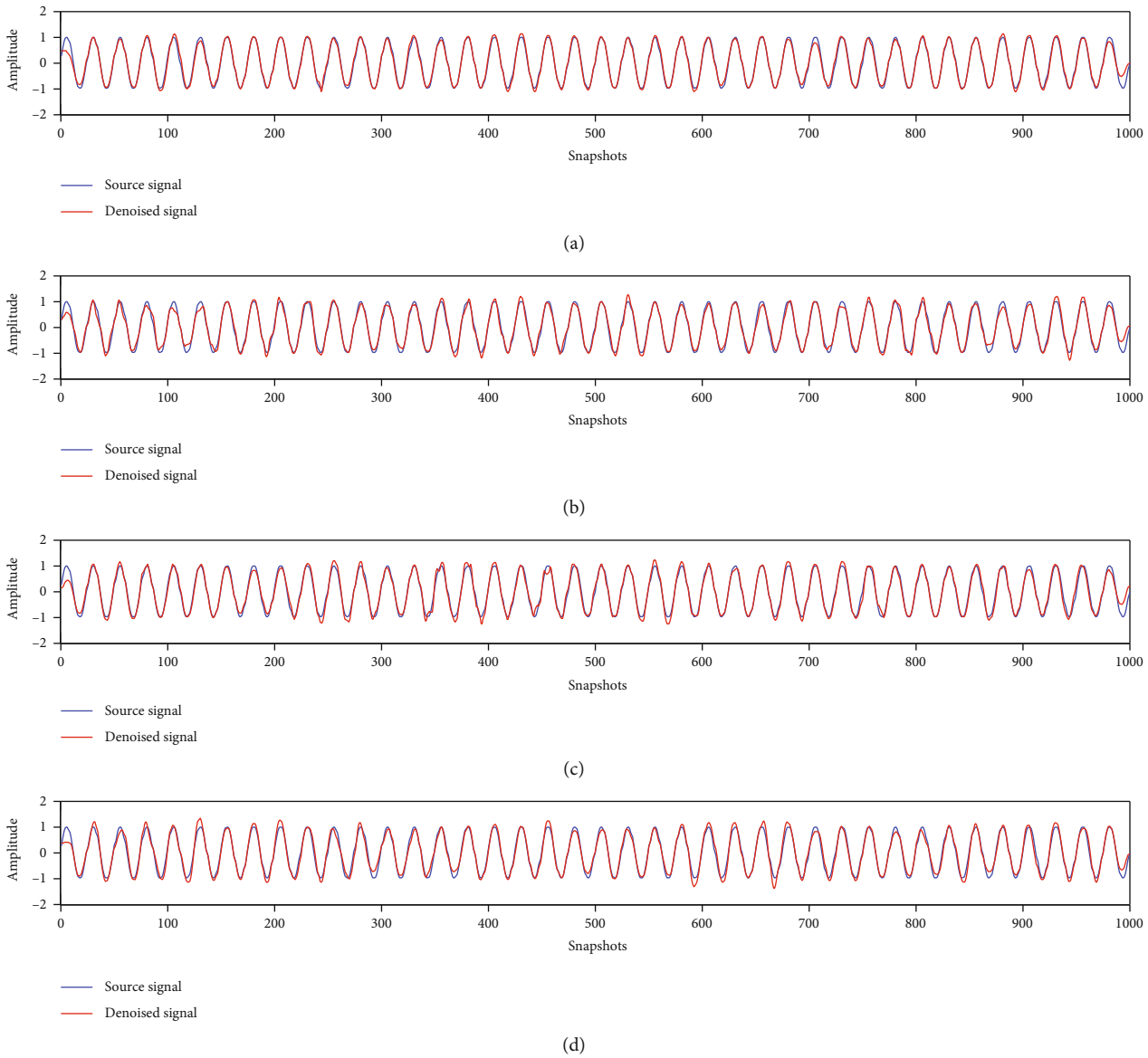

Figure 12: Denoised results of these four algorithms under 5 dB: (a) MVO-PSO-VMD-CC-WT; (b) MVO-VMD-CC-WT; (c) PSO-VMD-CC-WT; (d) VMD-CC-WT.

VMD-CC-WT, and MVO-PSO-VMD-CC-WT are also independently run 30 times, respectively. The average SNRs and RMSEs are shown in Table 3.

From Table 3, it can be seen that MVO-PSO-VMD-CC-WT with different decibels has the least RMSE and the highest SNR among these five algorithms: SNR 4.3433 and RMSE 0.4293 under -10 dB; SNR 9.0947 and RMSE 0.2236 under -5 dB; SNR 13.8305 and RMSE 0.1440 under 0 dB; SNR 16.9478 and RMSE 0.1005 under 5 dB; SNR 20.1053 and RMSE 0.0695 under 10 dB. For the same decibels, according to the increasing of SNRs or the decreasing of RMSEs, the order of five algorithms in Table 3 is VMD-CC-WT, PSO-VMD-CC-WT, MVO-VMD-CC-WT, MVO-PSO-PSE-VMD-CC-WT, and MVO-PSO-VMD-CC-WT. And we also observe that SNRs are increasing and RMSEs are decreasing with the noise decibel increasing. Therefore, the results obtained from Table 3 show that MVO-PSO-VMD-CC-WT is superior to VMD-CC-WT, PSO-VMD-CC-WT, MVO-VMD-CC-WT, and MVO-PSO-PSE-VMD-CC-WT in the mixed frequency simulated denoising experiment.

4.3. Experimental Results. In this section, two simulated experiments are given to verify the validation of MVO-PSO-VMD-CC-WT by comparison with VMD-CC-WT, PSO-VMD-CC-WT, MVO-VMD-CC-WT, and MVO-PSO-PSE-VMD-CC-WT. Figures 2–13 show that the denoised signals under different noise-added decibels by VMD-CC-WT, PSO-VMD-CC-WT, MVO-VMD-CC-WT, and MVO-PSO-VMD-CC-WT match the noise-free source signals, where the denoised signals under different noise-added decibels by MVO-PSO-VMD-CC-WT match the noise-free source signals optimally. According to RMSE and SNR, MVO-PSO-VMD-CC-WT outperforms VMD-CC-WT, PSO-VMD-CC-WT, and MVO-VMD-CC-WT.

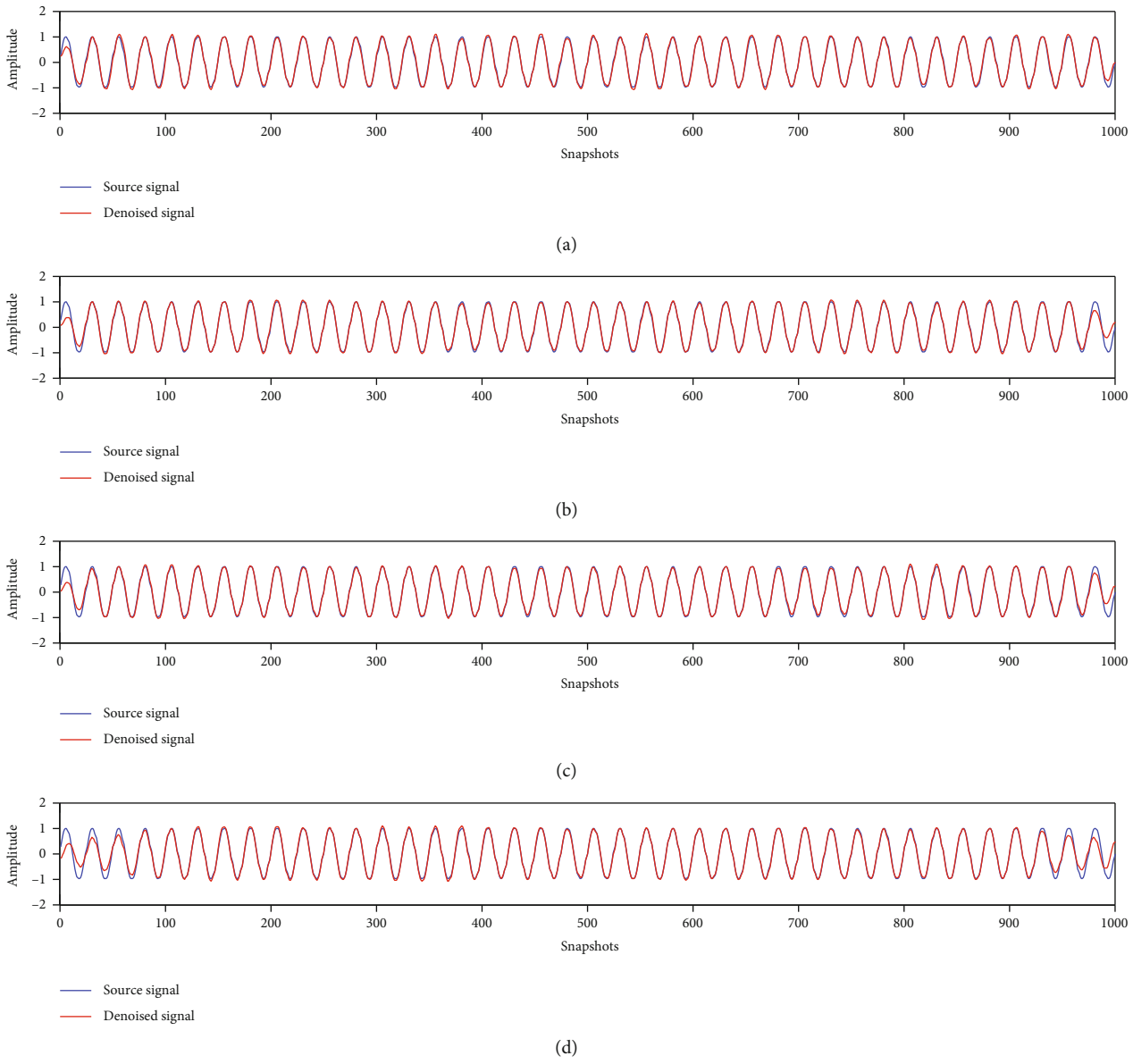

Figure 13: Denoised results of these four algorithms under 10 dB: (a) MVO-PSO-VMD-CC-WT; (b) MVO-VMD-CC-WT; (c) PSO-VMD-CC-WT; (d) VMD-CC-WT.

Further, the fitness function RMSE of MVO-PSO-VMD-CC-WT is replaced with PSE, and thus, MVO-PSO-PSE-VMD-CC-WT is established. The comparable results show that the proposed MVO-PSO-VMD-CC-WT is better than MVO-PSO-PSE-VMD-CC-WT. Therefore, the proposed MVO-PSO-PSE-VMD-CC-WT in this paper with the fitness function RMSE is suitable for the simulated signal denoising.

5. Lake Experiments

In this paper, the measured data used are derived from Fenji experiments conducted by North University of China in 2011 and 2014 in Fenhe Reservoir 2, respectively. In this section, we apply the above proposed MVO-PSO-VMD-CC-WT to perform the signal denoising on these measured data.

5.1. Experiment 1: The Measured Experimental Data of Fenji in 2011. In the experiment, a MEMS vector hydrophone with 4-element line array where 1-meter distance was between two adjacent array elements was fixed on the shore, and the acoustic signal emission transducer was placed on the tugboat. Then, the hydrophone is placed at 6 meters underwater, and the transducer was used to transmit signals after anchoring in different positions by the tug, and then, the data is collected. These Fenji measured data with transmitting signal frequency of 331 Hz are chosen to verify the validation of MVO-PSO-VMD-CC-WT. And these Fenji measured data are obtained from X road and Y road of 1# and 2# MEMS vector hydrophones in 2011, respectively. In this section, the measured data with the length of 1000 snapshots obtained from X road and Y road of 1# and 2# MEMS vector hydrophones in 2011 are randomly taken for granted.

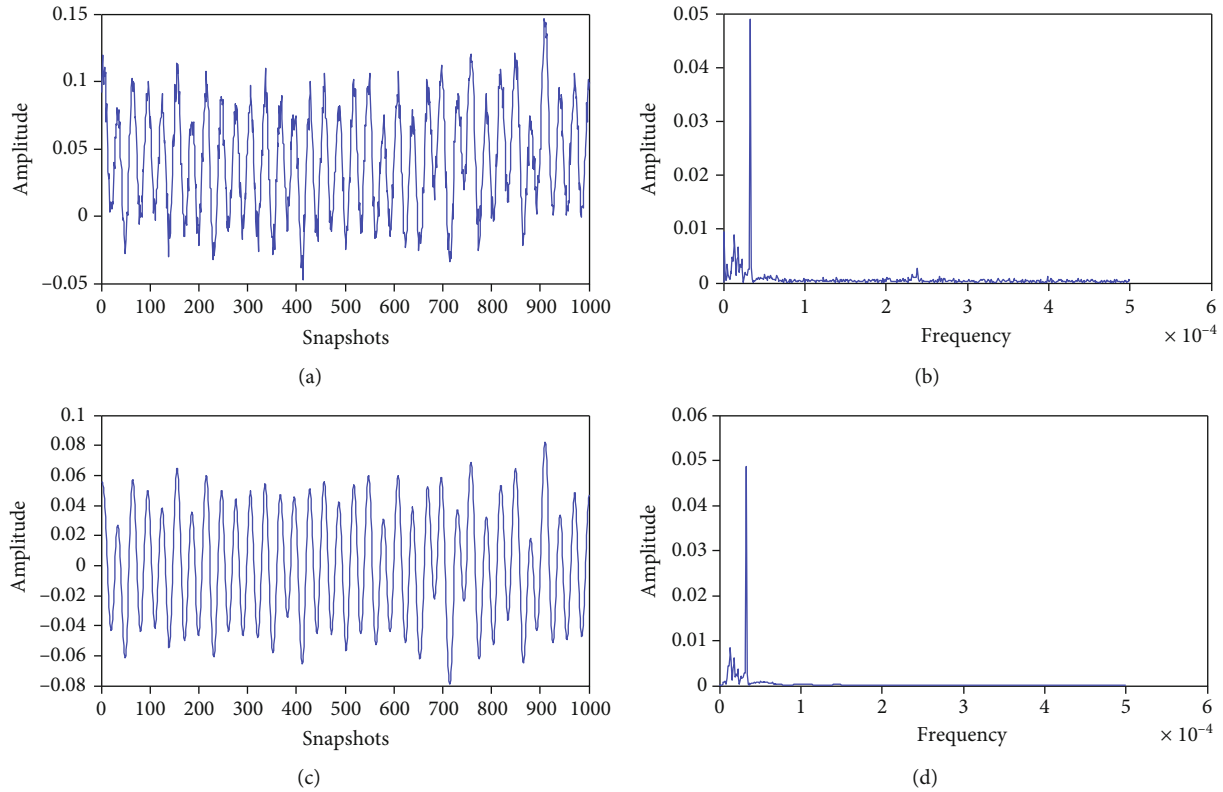

Figure 14: X road signal of 1# vector hydrophone (2011.10). (a) Noisy measured signal. (b) Frequency spectrum of noisy measured signal. (c) Denoised measured signal. (d) Frequency spectrum of denoised measured signal.

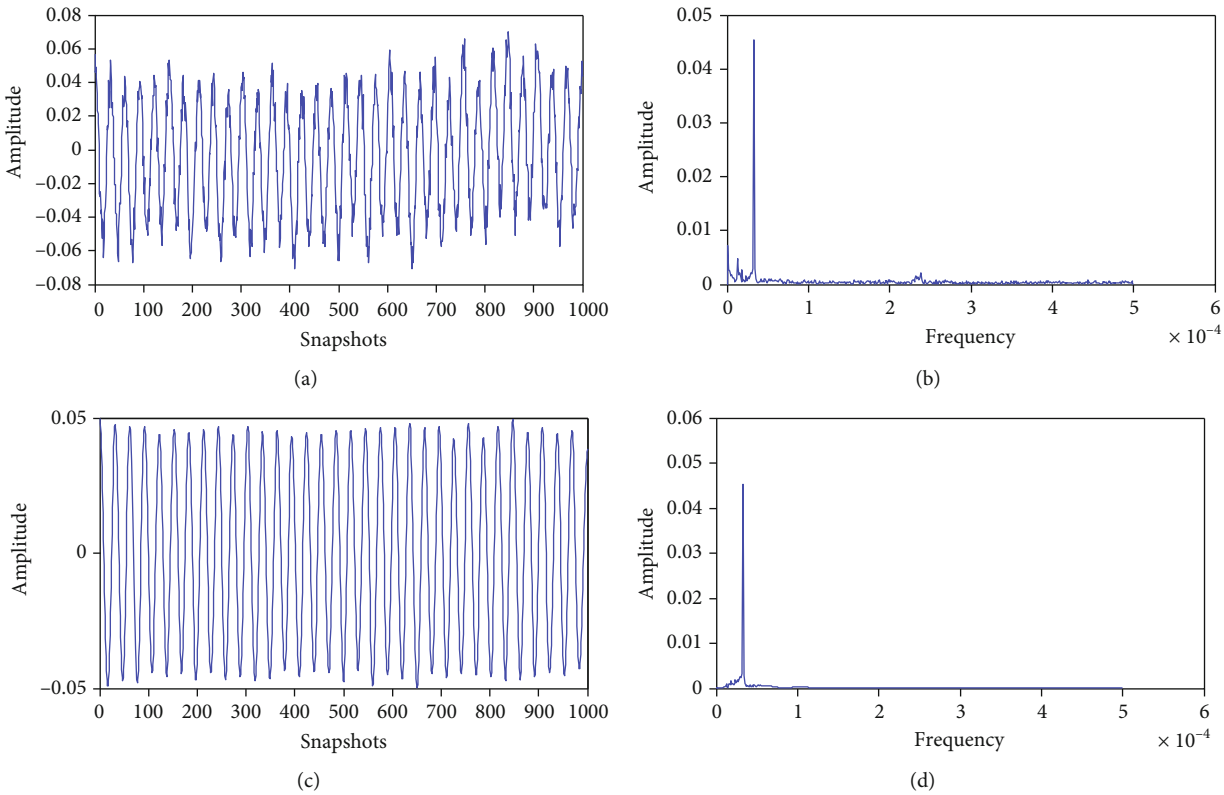

Figure 15: Y road signal of 1# vector hydrophone (2011.10). (a) Noisy measured signal. (b) Frequency spectrum of noisy measured signal. (c) Denoised measured signal. (d) Frequency spectrum of denoised measured signal.

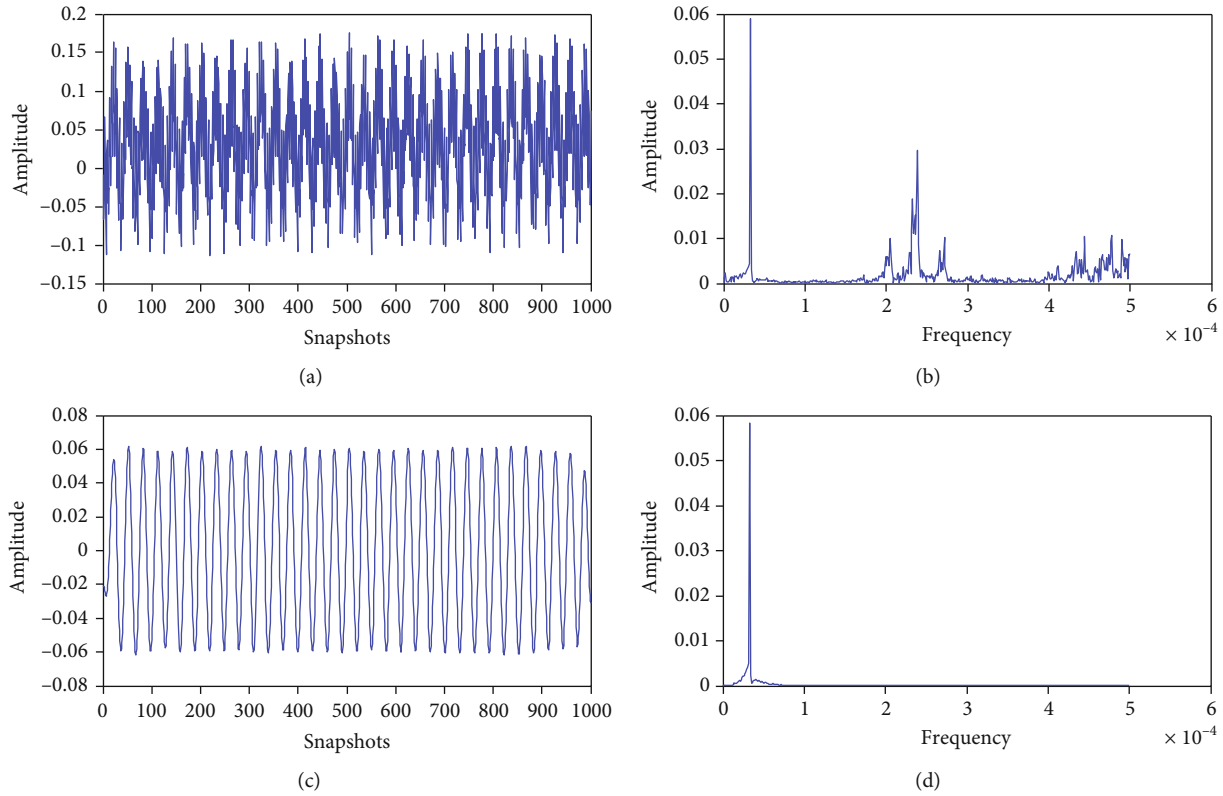

Figure 16: X road signal of 2# vector hydrophone (2011.10). (a) Noisy measured signal. (b) Frequency spectrum of noisy measured signal. (c) Denoised measured signal. (d) Frequency spectrum of denoised measured signal.

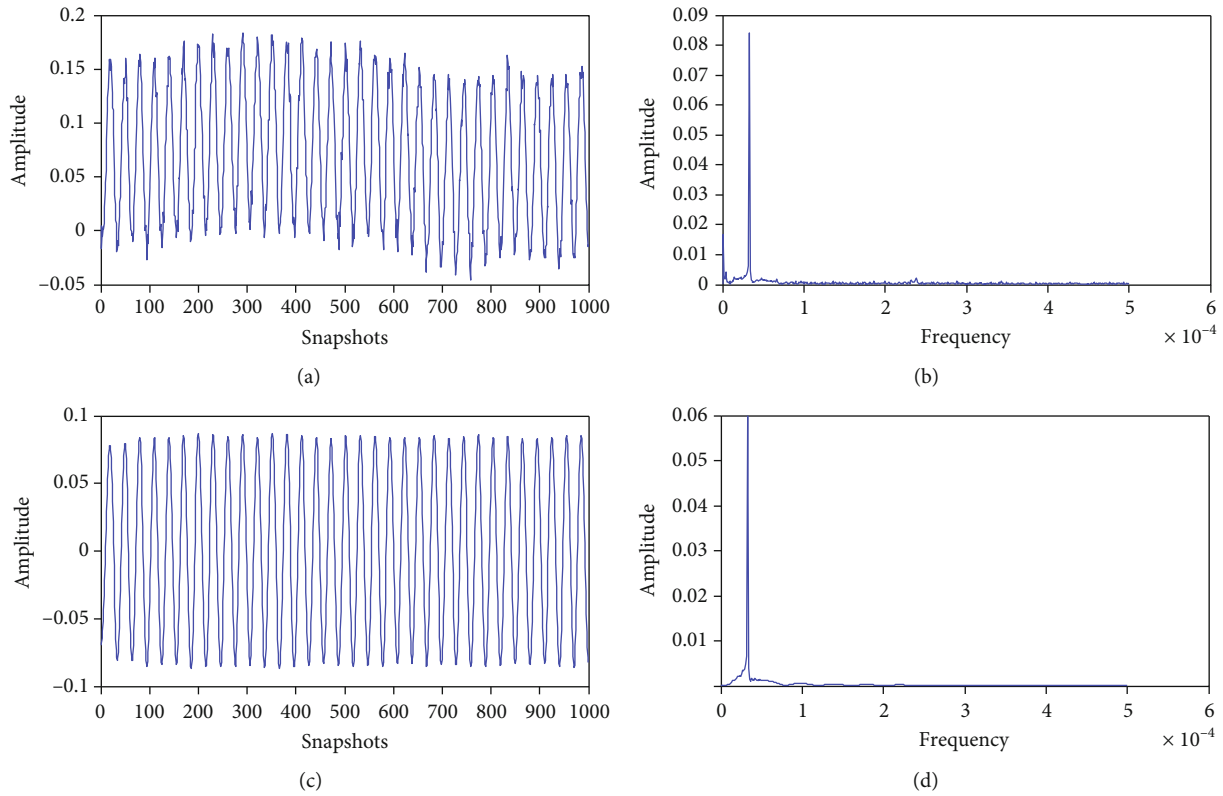

Figure 17: Y road signal of 2# vector hydrophone (2011.10). (a) Noisy measured signal. (b) Frequency spectrum of noisy measured signal. (c) Denoised measured signal. (d) Frequency spectrum of denoised measured signal.

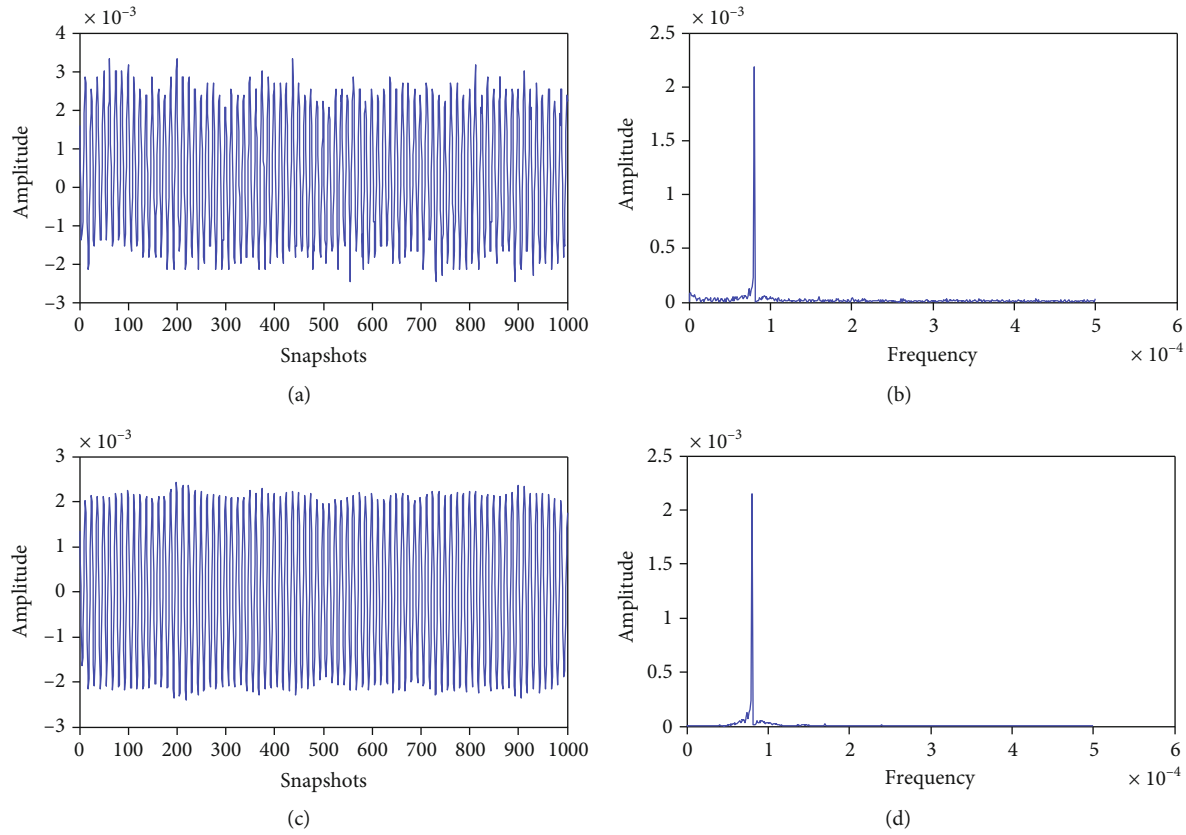

Figure 18: X road of 2# hydrophone with 800 Hz (2014.9). (a) Noisy measured signal. (b) Frequency spectrum of noisy measured signal. (c) Denoised measured signal. (d) Frequency spectrum of denoised measured signal.

Figures 14–17 are the measured signals and their corresponding spectra and also show the noised signals of the measured signals and their corresponding spectra by MVO-PSO-VMD-CC-WT, where Figures 14 and 15 are obtained from X road and Y road of 1# vector hydrophone, respectively, and Figures 16 and 17 are obtained from X road and Y road of 2# vector hydrophone, respectively.

From (a) and (b) in Figures 14–17, we can observe that there are some glitches in the frequency spectra of the signals, which shows that there exists a small amount of noise in the signal and the signals have relative fluctuations. In particular, from (a) and (b) in Figure 16, we can observe that there are a large number of sharp protrusions in the frequency spectra of the signals, which indicates that the signal is mixed with a large number of high-frequency noise and the signal has been seriously distorted.

he (c) and (d) in Figures 14–17 are the denoised signals and their corresponding frequency spectra obtained MVO-PSO-VMD-CC-WT. It is observed that the denoised signals preserve the basic characteristics of the noise-free source signals and the baseline drifts are corrected to the zero level. Thus, the sharp noises are eliminated effectively by MVO-PSO-VMD-CC-WT and the distortions of the denoised signals are improved, which make the denoised signals smoother and neater. And from (d) in Figures 14–17, we also observe that the energy of the signals is hardly no loss.

5.2. Experiment 2: The Measured Experimental Data of Fenji in 2014. In the experiment, MEMS vector hydrophone with 2-element line array where there was 0.5-meter distance between two adjacent array elements was fixed on the shore, and the acoustic signal emission transducer was placed on the tugboat. There was the distance of 10 meters between the sound source and the MEMS vector hydrophone. And the transducer was used to transmit signals, and then, Fenji measured data was collected.

In this paper, these Fenji measured data in September 2014 with transmitting signal frequency of 800 Hz and 1000 Hz are chosen to verify the validation of MVO-PSO-VMD-CC-WT. And these Fenji measured data are obtained from X road and Y road of 2# MEMS vector hydrophones in 2014, respectively. In this section, the measured data with the length of 1000 snapshots obtained from X road and Y road of 2# MEMS vector hydrophones in 2014 are randomly taken for granted.

Figures 18 and 19 are the measured signals and their corresponding spectra, respectively, and also show the noised signals of the measured signals and their corresponding spectra by MVO-PSO-VMD-CC-WT, respectively. Figure 18 is X road of 2# hydrophone with 800 Hz, and Figure 19 is Y road of 2# hydrophone with 1000 Hz.

From (a) and (b) in Figure 18, we can observe that there are a large number of glitches in X road of 2# vector

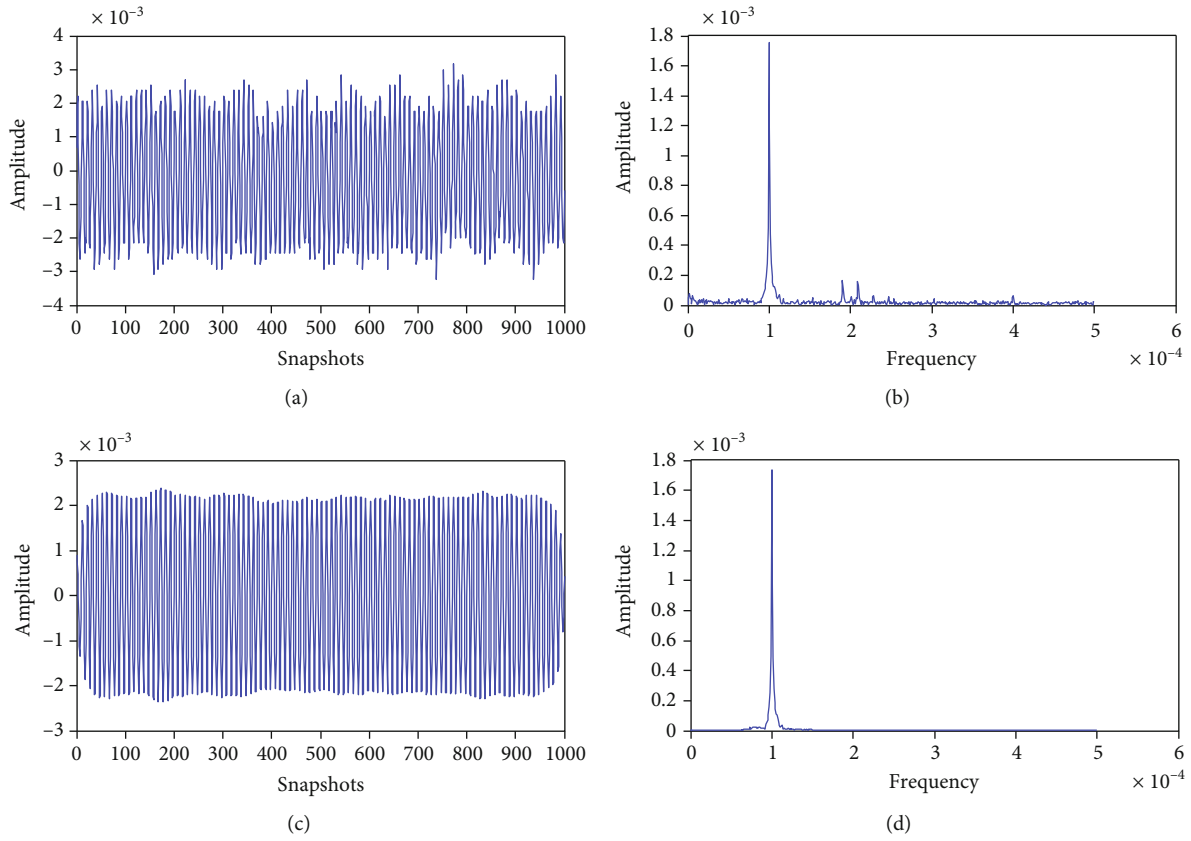

Figure 19: Y road of 2# hydrophone with 1000 Hz (2014.9). (a) Noisy measured signal. (b) Frequency spectrum of noisy measured signal. (c) Denoised measured signal. (d) Frequency spectrum of denoised measured signal.

hydrophone with 800 Hz frequency, which indicates that there is a large amount of noise in the signal and there exists the relative distortion in the signal. From (a) and (b) in Figure 19, we can observe that there are some glitches in the left half of frequency spectrum in X road of 2# vector hydrophone with 1000 Hz frequency, which indicates that the signal is mixed with low-frequency noise, and there are some sharp protrusions in the right half of the frequency spectrum, which indicates that the signal is mixed with a lot of high-frequency noise and that high-frequency noise has great interference and leads to severe distortion of the signal.

The (c) and (d) in Figures 18 and 19 are the denoised signals and their corresponding frequency spectra obtained from Figures 18(a) and 19(a) by using MVO-PSO-VMD-CC-WT. We observe that the denoised signals preserve the basic characteristics of the noise-free source signal and the baseline drifts are corrected to the zero level. Thus, the sharp noises are eliminated effectively by MVO-PSO-VMD-CC-WT and the distortions of the denoised signals are improved, which make the denoised signals smoother and neater.

5.3. Experimental Results. The above two experimental results show that the MVO-PSO-VMD-CC-WT proposed in this paper can effectively eliminate the noise of the measured signals, can well retain the basic characteristics of the sound source signal, and can make the baseline drifts be corrected, which gives an inspiration in the actual denoising applications.

6. Conclusion

In this paper, the proposed MVO-PSO algorithm is used to optimize the number k of IMFs obtained by VMD and the penalty factor α and the optimized VMD is obtained. Thus, the hybrid denoising algorithm MVO-PSO-VMD-CC-WT based on WT denoising and VMD optimized by MVO-PSO algorithm in terms of CC judgement is proposed to perform the denoising of the signal mixed with noise received from MEMS vector hydrophone. Two simulated experiments show that MVO-PSO-VMD-CC-WT can be able to effectively perform denoising and has the least RMSE and the highest SNR and that MVO-PSO-VMD-CC-WT outperforms the other compared algorithm. Further, MVO-PSO-VMD-CC-WT is applied to perform denoising of the Fenji measured signal, and the denoised results show that MVO-PSO-VMD-CC-WT has an ability in signal denoising and the baseline drift corrected and with a simple principle and fast calculation speed and has certain practical research significance.

7. Discussion

In the wavelet threshold (WT) denoising method, the section of the threshold function is important. Currently, the hard threshold function and the soft threshold function are the most widely applicable in many fields. It is found that the hard threshold function is discontinuous at the threshold

point, which makes the estimated signal produce additional oscillation to a certain extent. Compared with the hard threshold function, the soft threshold function avoids this problem, and the processing result is relatively smooth. However, the deviation between the wavelet estimation coefficient after soft threshold and the wavelet coefficient of the input noisy signal is always inevitable, which affects the approximation degree between the denoised signal and the source signal. For this reason, many scholars improve the threshold function to improve the effect of wavelet threshold denoising. In this paper, the soft threshold denoising method is chosen. In the later researches, the threshold function needs to be improved further. Although variational mode decomposition (VMD) overcomes the disadvantages of EMD, EEMD, and CEEMD and has a solid theoretical foundation and can better solve modal aliasing problems, the number of IMFs obtained by VMD and the penalty factor need to be set up in advance. Therefore, the appropriate parameters are the essential key in VMD for signal decomposition. We apply the swarm intelligence algorithm to optimize the number of IMFs obtained by VMD and the penalty factor and obtain the optimized VMD. Further, the combination of WT, the optimized VMD, and correlation coefficient (CC) is able to perform the signal denoising and overcome the disadvantages of VMD and WT, whose performance is superior to the two individual methods.

In the future, according to the foundation of MVO-PSO-VMD-CC-WT proposed in the paper, we can propose more and more hybrid algorithms to be applied to perform signal denoising.

Data Availability

In this paper, the measured data used are derived from Fenji experiments conducted by North University of China in 2011 and 2014 in Fenhe Reservoir 2, respectively.

Conflicts of Interest

The authors declare no financial conflicts of interest.

Acknowledgments

This work was supported in part by Shanxi Scholarship Council of China (Grant No. 2020-104), Shanxi Natural Science Foundation (Grant numbers 201801D121026 and 201701D221121), National Nature Science Foundation of China (Grant Nos. 61774137, 51875535, and 61927807), and Key Research and Development Projects of Shanxi Province (Grant number 201903D121156).

References

[1] L. Salvatore, N. Gallo, M. L. Natali et al., "Marine collagen and its derivatives: versatile and sustainable bio-resources for healthcare," *Materials Science and Engineering: C*, vol. 113, article 110963, 2020.

[2] L. Hammar, S. Molander, J. Pålsson et al., "Cumulative impact assessment for ecosystem-based marine spatial planning," *Science of the Total Environment*, vol. 734, article 139024, 2020.

[3] Z. Guojun, Q. Xu, Z. Cong, C. Shang, and S. Yang, "Optimization of shell packaging for cilium MEMS bionic vector hydrophone," *Sensors and Actuators A: Physical*, vol. 306, article 111969, 2020.

[4] Z. Wang, W. Zhao, W. Du, N. Li, and J. Wang, "Data-driven fault diagnosis method based on the conversion of erosion operation signals into images and Convolutional Neural Network," *Process Safety and Environmental Protection*, vol. 149, pp. 591–601, 2021.

[5] M. J. Corinthios, "A fast Fourier transform for high-speed signal processing," *IEEE Transactions on Computers*, vol. C-20, no. 8, pp. 843–846, 1971.

[6] M. Portnoff, "Time-frequency representation of digital signals and systems based on short-time Fourier analysis," *IEEE Transactions on Acoustics, Speech, and Signal Processing*, vol. 28, no. 1, pp. 55–69, 1980.

[7] Y. Zhang, K. Xing, R. Bai, D. Sun, and Z. Meng, "An enhanced convolutional neural network for bearing fault diagnosis based on time-frequency image," *Measurement*, vol. 157, article 107667, 2020.

[8] X.-G. Shao, A. K.-M. Leung, and F.-T. Chau, "Wavelet: a new trend in chemistry," *Accounts of Chemical Research*, vol. 36, no. 4, pp. 276–283, 2003.

[9] M. Schimmack and P. Mercorelli, "A structural property of the wavelet packet transform method to localise incoherency of a signal," *Journal of the Franklin Institute*, vol. 356, no. 16, pp. 10123–10137, 2019.

[10] M. Schimmack and P. Mercorelli, "An on-line orthogonal wavelet denoising algorithm for high-resolution surface scans," *Journal of the Franklin Institute*, vol. 355, no. 18, pp. 9245–9270, 2018.

[11] P. Mercorelli, "Biorthogonal wavelet trees in the classification of embedded signal classes for intelligent sensors using machine learning applications," *Journal of the Franklin Institute*, vol. 344, no. 6, pp. 813–829, 2007.

[12] J. I. Salisbury and Y. Sun, "Assessment of chaotic parameters in nonstationary electrocardiograms by use of empirical mode decomposition," *Annals of Biomedical Engineering*, vol. 32, no. 10, pp. 1348–1354, 2004.

[13] F. Li, B. Zhang, S. Verma, and K. J. Marfurt, "Seismic signal denoising using thresholded variational mode decomposition," *Exploration Geophysics*, vol. 49, no. 4, pp. 450–461, 2018.

[14] M. S. Yakoub, S.-a. Selouani, B.-F. Zaidi, and A. Bouchair, "Improving dysarthric speech recognition using empirical mode decomposition and convolutional neural network," *EURASIP Journal on Audio, Speech, and Music Processing*, vol. 2020, no. 1, 2020.

[15] Y. Niu, J. Fei, Y. Li, and D. Wu, "A novel fault diagnosis method based on EMD, cyclostationary, SK and TPTSR," *Journal of Mechanical Science and Technology*, vol. 34, no. 5, pp. 1925–1935, 2020.

[16] Z. Wu and N. E. Huang, "Ensemble empirical mode decomposition: a noise-assisted data analysis method," *Advances in Adaptive Data Analysis*, vol. 1, no. 1, pp. 1–41, 2009.

[17] L. Chen, X. Li, X.-b. Li, and Z.-y. Huang, "Signal extraction using ensemble empirical mode decomposition and sparsity in pipeline magnetic flux leakage nondestructive evaluation," *The Review of Scientific Instruments*, vol. 80, no. 2, article 025105, 2009.

[18] J. R. Yeh, J. S. Shieh, and N. E. Huang, "Complementary ensemble empirical mode decomposition: a novel noise

enhanced data analysis method," *Advances in Adaptive Data Analysis*, vol. 2, no. 2, pp. 135–156, 2010.

[19] S. Zhu, X. Lian, L. Wei et al., "$PM_{2.5}$ forecasting using SVR with PSOGSA algorithm based on CEEMD, GRNN and GCA considering meteorological factors," *Atmospheric Environment*, vol. 183, pp. 20–32, 2018.

[20] K. Dragomiretskiy and D. Zosso, "Variational mode decomposition," *IEEE Transactions on Signal Processing*, vol. 62, no. 3, pp. 531–544, 2014.

[21] H. Hu, L. Zhang, H. Yan, Y. Bai, and P. Wang, "Denoising and baseline drift removal method of MEMS hydrophone signal based on VMD and wavelet threshold processing," *IEEE Access*, vol. 7, pp. 59913–59922, 2019.

[22] W. Liu, S. Cao, and Y. Chen, "Applications of variational mode decomposition in seismic time-frequency analysis," *Geophysics*, vol. 81, no. 5, pp. V365–V378, 2016.

[23] W. Liu, S. Cao, Z. Wang, X. Kong, and Y. Chen, "Spectral Decomposition for Hydrocarbon Detection Based on VMD and Teager–Kaiser Energy," *IEEE Geoscience and Remote Sensing Letters*, vol. 14, no. 4, pp. 539–543, 2017.

[24] W. Liu, S. Cao, Z. Wang, K. Jiang, Q. Zhang, and Y. Chen, "A novel approach for seismic time-frequency analysis based on high-order synchrosqueezing transform," *IEEE Geoscience and Remote Sensing Letters*, vol. 15, no. 8, pp. 1159–1163, 2008.

[25] R. Gu, J. Chen, R. Hong, H. Wang, and W. Wu, "Incipient fault diagnosis of rolling bearings based on adaptive variational mode decomposition and Teager energy operator," *Measurement*, vol. 149, p. 106941, 2020.

[26] H. Yang, L. Gao, and G. Li, "Underwater acoustic signal prediction based on MVMD and optimized kernel extreme learning machine," *Complexity*, vol. 2020, Article ID 6947059, 17 pages, 2020.

[27] Q. Xiao, J. Li, and Z. Zeng, "A denoising scheme for DSPI phase based on improved variational mode decomposition," *Mechanical Systems and Signal Processing*, vol. 110, pp. 28–41, 2018.

[28] C. Wang, H. Li, G. Huang, and J. Ou, "Early fault diagnosis for planetary gearbox based on adaptive parameter optimized VMD and singular kurtosis difference spectrum," *IEEE Access*, vol. 7, pp. 31501–31516, 2019.

[29] J. Bian, "Fault diagnosis of bearing combining parameter optimized variational mode decomposition based on genetic algorithm with 1.5-dimensional spectrum," *Journal of Propulsion Technology*, vol. 38, pp. 1618–1624, 2017.

[30] H. Yan, T. Xu, P. Wang, L. Zhang, H. Hu, and Y. Bai, "MEMS hydrophone signal denoising and baseline drift removal algorithm based on parameter-optimized variational mode decomposition and correlation coefficient," *Sensors*, vol. 19, no. 21, p. 4622, 2019.

[31] Z. Wang, N. Yang, N. Li, W. Du, and J. Wang, "A new fault diagnosis method based on adaptive spectrum mode extraction," *Structural Health Monitoring*, 2021.

[32] S. Mirjalili, S. M. Mirjalili, and A. Hatamlou, "Multi-verse optimizer: a nature-inspired algorithm for global optimization," *Neural Computing & Applications*, vol. 27, no. 2, pp. 495–513, 2016.

[33] Y. Zhou, Z. Zhao, and D. Cheng, "Cluster structure prediction via revised particle-swarm optimization algorithm," *Computer Physics Communications*, vol. 247, p. 106945, 2020.

[34] F. Karaaslan and S. Özlü, "Correlation coefficients of dual type-2 hesitant fuzzy sets and their applications in clustering analysis," *International Journal of Intelligent Systems*, vol. 35, no. 7, pp. 1200–1229, 2020.

[35] Y. Li, Y. Li, X. Chen, and J. Yu, "Research on ship-radiated noise denoising using secondary variational mode decomposition and correlation coefficient," *Sensors*, vol. 18, no. 2, p. 48, 2018.